A Model-Independent Data Assimilation (MIDA) module and its applications in ecology

Xin Huang[1,2], Dan Lu[3], Daniel M. Ricciuto[4], Paul J. Hanson[4], Andrew D. Richardson[1,2], Xuehe Lu[5], Ensheng Weng[6,7], Sheng Nie[8], Lifen Jiang[1], Enqing Hou[1], Igor F. Steinmacher[2], Yiqi Luo[1,2,9]

1 Center for Ecosystem Science and Society, Northern Arizona University, Flagstaff, AZ, USA

2 School of informatics, Computing, and Cyber Systems, Northern Arizona University, Flagstaff, AZ, USA

3 Computational Sciences and Engineering Division, Climate Change Science Institute, Oak Ridge National Laboratory, Oak Ridge, TN, USA

4 Environmental Sciences Division, Climate Change Science Institute, Oak Ridge National Laboratory, Oak Ridge, TN, USA

5 International Institute for Earth System Science, Nanjing University, Nanjing, China

6 Center for Climate Systems Research, Columbia University, New York, USA

7 NASA Goddard Institute for Space Studies, New York, USA

8 Key Laboratory of Digital Earth Science, Aerospace Information Research Institute, Chinese Academy of Sciences, Beijing, China

9 Department of Biological Sciences, Northern Arizona University, Flagstaff, AZ, USA

Correspondence to: Xin Huang (xh59@nau.edu)

ABSTRACT

Models are an important tool to predict Earth system dynamics. An accurate prediction of future states of ecosystems depends on not only model structures but also parameterizations. Model parameters can be constrained by data assimilation. However, applications of data assimilation to ecology are restricted by highly technical requirements such as model-dependent coding. To alleviate this technical burden, we developed a model-independent data assimilation (MIDA) module. MIDA works in three steps including data preparation, execution of data assimilation, and visualization. The first step prepares prior ranges of parameter values, a defined number of iterations, and directory paths to access files of observations and models. The execution step calibrates parameter values to best fit the observations and estimates the parameter posterior distributions. The final step automatically visualizes the calibration performance and posterior distributions. MIDA is model independent and modelers can use MIDA for an accurate and efficient data assimilation in a simple and interactive way without modification of their original models. We applied MIDA to four types of ecological models: the data assimilation linked ecosystem carbon (DALEC) model, a surrogate-based energy exascale earth system model: the land component (ELM), nine phenological models and a stand-alone biome ecological strategy simulator (BiomeE). The applications indicate that MIDA can effectively solve data assimilation problems for different ecological models. Additionally, the easy implementation and model-independent feature of MIDA breaks the technical barrier of ~~black-box~~ applications of data-model fusion in ecology. MIDA facilitates the assimilation of various observations into models for uncertainty reduction in ecological modeling and forecasting.

Keywords:

Parameter uncertainty quantification, Data assimilation, Modules, Ecological models

1. Introduction

Ecological models require a large number of parameters to simulate biogeophysical and biogeochemical processes (Bonan, 2019; Ciais et al., 2013; Friedlingstein et al., 2006), and specify model behaviors (Luo et al., 2016; Luo and Schuur, 2020). Parameter values in ecological models are mostly determined in some *ad hoc* fashions (Luo et al., 2001), leading to considerable biases in predictions (Tao et al., 2020). The situation becomes even worse when more detailed processes are incorporated into models (De Kauwe et al., 2017; Lawrence et al., 2019). Data assimilation (DA), a statistically rigorous method to integrate observations and models, is gaining increasing attention for parameter estimation and uncertainty evaluation. It has been successfully applied to many ecological models (Fox et al., 2009; Keenan et al., 2012; Richardson et al., 2010; Safta et al., 2015; Wang et al., 2009; Williams et al., 2005; Zobitz et al., 2011). However, almost all those DA studies require model-dependent, invasive coding (Walls et al., 2005). This requires a DA algorithm to be programmed for a specific model. Such model-dependent coding creates a large technical barrier for ecologists to use DA to solve prediction and uncertainty quantification problems in ecology. Thus a model-independent DA toolkit is required to facilitate the use of DA technique in ecology.

DA is a powerful approach to combine models with observations and can be used to improve ecological research in several ways (Luo et al., 2011). First, DA can be used for parameter estimation (Bloom et al., 2016; Hararuk et al., 2015; Hou et al., 2019; Ise and Moorcroft, 2006; Ma et al., 2017; Ricciuto et al., 2011; Scholze et al., 2007). It enables the optimization of parameter values across sites, time and treatments (Li et al., 2018; Luo and Schuur, 2020). For example, Hararuk and his colleagues applied DA to a global land model and substantially improved the explanability of the global variation in soil organic carbon (SOC)

from 27% to 41% (Hararuk et al., 2014). When DA was combined with deep learning to improve spatial distributions of estimated parameter values, for example, the Community Land Model version 5 (CLM5) predicted the SOC distribution in the US continent with much higher R^2 of 0.62 than CLM5 with default parameters (R^2 = 0.32) (Tao et al., 2020). Second, DA can be used to select alternative model structures to better represent ecological processes (Liang et al., 2018; Van Oijen et al., 2011; Shi et al., 2018; Smith et al., 2013; Williams et al., 2009). In the study by Liang et al. (2018), DA was used to evaluate four models. Aand a two-pool interactive model was selected after DA to best represent SOC decomposition with priming ~~(Liang et al., 2018)~~. Additionally, DA can be applied ~~for data-worth analysis~~ to locate the most informative data to reduce uncertainty, thus guiding the sensor network design. (Keenan et al., 2013; Raupach et al., 2005; Shi et al., 2018; Williams et al., 2005). One DA study at Harvard Forest (Keenan et al., 2013) indicated that only a few data sources contributed to the significant reduction in parameter uncertainty. In spite of powerful applications of DA to ecological research, computational cost is a major hurdle, especially with complex models. Fer et al. (2018) developed a Bayesian model emulation to reduce the time cost of DA from 112h to 6h with the simplified Photosynthesis and Evapotranspiration model. Overall, DA is essential for ecological modeling and forecasting (Jiang et al., 2018) and is helpful for evaluation of different inversion methods (Fox et al., 2009).

Applications of traditional DA to ecological research require highly technical skills of users. A successful DA application usually involves model-dependent coding to integrate observations into models. This requires users to have knowledge about model programing. For example, if a complex model (e.g., the community land model) is used in DA, users need to know the programming language (e.g., Fortran) of the model and its internal content to write DA algorithm into the model source code before DA can be conducted. The learning curve for model

programing is steep for general ecologists. Furthermore, users often need to update the programming knowledge when a different model is used in DA. For example, scientists who implemented the DA algorithm coded in MATLAB (Xu et al., 2006) to an ecosystem carbon cycle model programmed in Fortran (e.g., TECO) need to understand both MATLAB and Fortran (Ma et al., 2017). Moreover, DA often involves reading observation files about a specific study site. As a result, users usually have to update the codes of model-dependent DA to read new observations from every new study site.

A number of tools have been developed to facilitate DA applications (Table 1) but many of them are model dependent, such as the Carbon Cycle Data Assimilation Systems (CCDAS) (Rayner et al., 2005; Scholze et al., 2007), the Carbon Data Model Framework (CARDAMOM) (Bloom et al., 2016), ~~and~~ the Ecological Platform for Assimilating Data (EcoPAD) into model ~~data assimilation systems~~ (Huang et al. 2019) and Predictive Ecosystem Analyzer (PEcAn) (LeBauer et al., 2013). These tools combine DA algorithms with a specific model. For example, CCDAS specified the DA algorithm to the Biosphere Energy Transfer Hydrology (BETHY) model (Rayner et al., 2005). The hardcoding feature of aforementioned tools make them inflexible to be applied to different models.

There are some model independent DA tools that are not tailored to a specific model, such as Data Assimilation Research Testbed (DART) (Anderson et al., 2009), the open Data Assimilation library (openDA) (Ridler et al., 2014), the Parallel Data Assimilation Framework (PDAF) (Nerger and Hiller, 2013) and Parameter Estimation & Uncertainty Analysis software suit (PEST) (Doherty, 2004).

However, these model-independent tools suffer from some limitations for a general and flexible DA application. For example, openDA requires users to code three functions to initialize

a Java class (Ridler et al., 2014) (Table 1). DART enables incorporating a new model through a range of interfaces (Anderson et al., 2009). It has been successfully applied to atmospheric and oceanic models with currently available interfaces (Anderson et al., 2009; Raeder et al., 2012) and recently to the community land model (Fox et al., 2018). It is likely that users may need to prepare new interfaces for new ecological models to use DART. DART and PDAF adopted the Ensemble Kalman Filter (EnKF) method (Evensen, 2003), which may makes it difficult to obey mass conservation for biogeochemical models. This is because the parameter values estimated by EnKF change each time when new data sets are assimilated (Allen et al., 2003; Gao et al., 2011; Trudinger et al., 2007). The ~~disruptive~~ sudden changes in estimated parameter values at time points when data are assimilated by EnKF usually do not reflect reality of biogeochemical cycles in the real world. PEST utilizes Levenberg-Marquardt method (Levenberg, 1944) which is a local optimization method for parameter estimation. If the relationship between simulation outputs and parameters are highly nonlinear, which is common in ecological models, this method may trap into a locally optimization solution (Doherty, 2004).

In this work, we developed a model-independent DA module (MIDA) to enable a general and flexible application of DA in ecology. MIDA was designed as a highly modular tool, independent of specific models, and friendly to users with limited programming skills and/or technical knowledge of DA algorithms. Additionally, MIDA implemented advanced Markov Chain Monte Carlo (MCMC) algorithms for DA analysis which can accurately quantify the parameter uncertainty with informative posterior distribution. The anticipated user community in this initial phase of MIDA development is the biogeochemical modelers who are looking for appropriate parameter estimation methods. In the following Section 2, we first introduce the development details of MIDA and its usage. In Section 3, we demonstrate the application of

MIDA to four different types of ecological models. In Section 4, we discuss the strengths and weaknesses of MIDA in ecological modelling and lastly we give our concluding remarks in Section 5.

2. Model-independent data assimilation (MIDA)

2.1 Bayes's theorem and DA ~~algorithm~~

Based on Bayes' theorem, DA is a statistical approach ~~algorithm~~ to constrain parameter values and estimate their posterior density distributions through assimilating observations into a model. The posterior density distributions $p(C|Z)$ of parameters C for a given observation Z can be obtained from *prior* ~~parameter~~density distributions $p(C)$ and the likelihood function $p(Z|C)$:

$$p(C|Z) \propto p(Z|C)p(C) \quad (1)$$

The *prior* density ~~function~~distribution $p(C)$ is assumed as a uniform distribution over the parameter range. And the likelihood function is negatively proportional to a cost function, J as:

$$p(Z|C) \propto exp(-J) \quad (2)$$

The cost function measures the misfit between simulation outputs and observations and is described in more detail in section 2.4. The posterior density distributions $p(C|Z)$ is estimated from sampling -parameter values to maximize the likelihood function $p(Z|C)$ or minimize the cost function *J*. DA usually uses a sampling technique, such as Markov chain Monte Carlo (MCMC) in this MIDA. The MCMC algorithm successively generates a new set of parameter values from the prior parameter ranges and requires model run with these new parameter values. Then the cost function is calculated to determine whether this new set of parameter values will be accepted or not according to the Metropolis-Hastings criterion (see more description in section 2.4). All accepted parameter values are used to generate posterior distributions where the

distinctive mode indicates the parameter uncertainty is well constrained. Meanwhile, we derive maximum likelihood estimates (MLEs) of parameters from the posterior density distributions.

MIDA realizes model-independent Bayesian-based DA to estimate posterior density distributions and MLEs of parameters via data exchanges between a given model and DA algorithm.

~~This algorithm successively generates a new set of parameter values and requires model run with these new parameter values. Then the misfit between model simulation outputs and observations is calculated to determine whether this new set of parameter values will be accepted or not. The previously accepted parameter values help to generate new parameter values in the next iteration. Each iteration incorporates a model-dependent data exchange to transfer parameter values, model outputs, observations, etc. between DA algorithm and the model. Traditional DA requires implementing these data exchanges through model-specific programming into model code. As a result, a DA application inevitably involves intrusive modification of the original model.~~

2.2 An overview of MIDA

MIDA ~~(https://github.com/Celeste-Huang/MIDA, last access: Feb 2021)~~ is a module that allows for automatic implementation of data assimilation without intrusive modification or coding of the original model (https://doi.org/10.5281/zenodo.4762725, last access: May 2021). Its workflow includes three steps: data preparation, execution of data assimilation, and visualization (Fig. 1). Step 1 (data preparation) is to establish the standardized data exchange between DA algorithm and the model. Step 2 (execution of data assimilation) is to run DA as a black box independent of the model. Step 3 (visualization) is to diagnose parameter uncertainty after DA. The modularity of the 3-step workflow is designed to enable MIDA for a rapid DA application and adaption to a

new model. In the following, we introduce the three-step workflows of MIDA, its technical implementation and usage in detail.

2.3 Step 1: Data preparation

Step 1 is designed to initialize data exchange to transfer parameter values, model outputs, observations and their variances between DA algorithm and the model to be used. Four types of information are required either from interactive input or by modifying the 'namelist.txt' file (Fig. 1, 2). The first type is about DA configuration, including the number of sampling series in DA and the working path where the outputs of DA will be saved. The number of a sampling series is essential in a DA task to define how many times parameter values are sampled to run the model. The second type of information is about parameter ranges and their covariance. The third is the model executable file. Finally, the fourth type is an output configuration file which contains the file paths of model outputs, observations, and their variance. This file also instructs how to read model outputs and compare each output with corresponding observation.

Traditional DA requires users to modify the code of model to incorporate the process of data exchange between DA algorithm and the model. Therefore, the program of data exchange in traditional DA is model-specific and users need to repeat such program when a new model comes. In MIDA, the process of data exchange calls a model executable file which hides ~~hinders~~ the details of model code. When applied to a new model, MIDA only requires users to provide a different model executable file in the 'namelist.txt' file and does not involve any additional coding in either the model or MIDA. Thus, MIDA lowers the technical barrier for general ecologists to conduct DA.

Traditional DA usually preset the number of parameters and the model outputs according to a specific model before initializing the data exchange. This is because data exchange between DA algorithm and model uses memory to transfer~~s~~ items such as parameter values. Instead, MIDA organize~~s~~ items in data exchange using different files. Items in data exchange are decided by the data file loaded when MIDA is running. The number of parameter values, for example, will be decided after the file of parameter range is read in MIDA. Through modifying files, MIDA allows making efficient choices about the model-related items in data exchange. Thus, MIDA is highly flexible and modular for DA with different models.

Traditional DA also preset observation types in the data exchange according to a specific study before the data exchange. For example, if the traditional DA uses carbon flux observation, it cannot switch to satellite remote sensing products without additional coding. MIDA uses the concepts of object-orient programming (Mitchell and Apt, 2003) and dynamic initialization (Cline et al., 1998) in computer science to provide a homogenous way to create various observation types from a unified prototype class. A prototype class includes variables to store observations and their variance and functions (e.g., read from observation files). The values in variables are dynamically decided after the observation files are loaded when MIDA is running. Different observation types derive from the prototype class with a high degree of reusability of most functions. In such way, MIDA only requires users to provide different filenames of the observations to be integrated in DA. Therefore, MIDA is highly flexible and modular for DA to assimilate various observations.

2.4 Step 2: Execution of data assimilation

After the establishment of the standardized data exchange (step 1), step 2 is to run DA as a black box for users without knowledge of DA itself. Notwithstanding the black-box goal, this section provides a general description of DA below.

Data assimilation as a process integrates observations into a model to constrain parameters and estimate parameter uncertainties. Data assimilation usually uses some types of sampling algorithms, such as Markov chain Monte Carlo (MCMC), to generate posterior parameter distribution under a Bayesian inference ~~interference~~ framework (Box and Tiao, 1992). As mentioned in section 2.1, DA with MCMC algorithm estimates the posterior densit~~i~~y distributions through sampling to maximize likelihood function $p(Z|C)$ or minimize the misfit J between simulation outputs and observations. This version of MIDA uses MCMC algorithm implemented by the Metropolis-Hasting (MH) sampling method (Hastings, 1970; Metropolis et al., 1953)~~(Harrio et al., 2001)~~. The future version of MIDA could incorporate other data assimilation algorithms. Each iteration in the Metropolis-Hasting sampling includes a proposing phase and a moving phase. The proposing phase generates a new set of parameter values based on the starting point for the first iteration or current accepted parameter values in the following iterations. If parameter covariance (cov_{param}) is specified in step 1 on data preparation, this proposing phase will draw new parameter values ($C\sout{P}_{new}$) within the prior ranges from a Gaussian distribution $N(C\sout{P}_{old}, cov_{param})$ where $C\sout{P}_{old}$ is the predecessor set of parameter values. Without parameter covariance, new set of parameter values will be generated from a uniform distribution within the prior ranges (Xu et al., 2006).

The moving phase first calculates mismatches between observations and the model simulation with the new set of parameter values as a cost function (J_{new} in Eq.~~1~~3) (Xu et al. 2006):

$$J_{new} = \sum_{i=1}^{n} \frac{\sum_{t \in obs(Z_i)} [Z_i(t) - X_i(t)]^2}{2\sigma_i^2} \quad (13)$$

Formatted: Right

Where n is the number of observations, $Z_i(t)$ is the i[th] observation at time t, $X_i(t)$ is the corresponding simulation, σ_i^2 is the variance of the observations. The error is assumed to independently follow a Gaussian distribution. This new set of parameter values will be accepted if J_{new} is smaller than J_{old}, the cost function with the previous set of accepted parameter values, or the value, $\exp\left(-\frac{J_{new}}{J_{old}}\right)$, is larger than a random number selected from a uniform distribution from 0 to 1 according to the Metropolis criterion (Liang et al., 2018; Luo et al., 2011; Shi et al., 2018; Xu et al., 2006). Once the new set of parameter values is accepted, J_{new} becomes J_{old}. Those two phases of sampling will be iteratively executed until the number of sampling series set in step 1 on preparation of DA is reached. Finally, the posterior density distributions can be generated from all the accepted parameter values.

MIDA realizes the execution of data assimilation according to the procedure described above. First, MIDA uses a 'call' function to execute model simulations to get values of $X_i(t)$. Observations $Z_i(t)$ and their variance σ_i^2 are already provided via the standardized data exchange as described in step 1. Then, MIDA calculates J_{new} according to Eq. 3 equation 1 to decide the acceptance of the current parameter values used in this simulation. If accepted, MIDA saves this set of parameter values and associated J_{new} values in $CP_{accepted}$ and $J_{accepted}$ arrays respectively and triggers new proposing phrase based on this set of accepted parameter values. If not, MIDA discards this set of parameter values and generates another new set of parameter values. MIDA saves the new parameter values generated in the proposing phrase to "ParameterValue.txt", from which the model reads before execution of the next model simulation. MIDA repeats the proposing and moving phases until the number of sampling series

is reached. At the end, MIDA selects the best parameter values through maximum likelihood estimation and run model again using this set of values to get optimized simulation outputs $X_i(t)$. Then MIDA saves the arrays of accepted parameters, associated errors, maximum likelihood estimates (MLEs), and optimized state variables $X_i(t)$ to four files, "parameter_accepted.txt", "J_accepted.txt", "MLE.txt", and "OptimizedSimu.txt", respectively.

This execution of DA algorithm in MIDA enables users to conduct DA as a black box and is independent of any particular model.

2.5 Step 3: Visualization

Step 3 is to visualize the results of DA in step 2. The end products of DA are accepted parameter values, their associated J_{new} values, the maximum likelihood estimates, and optimized simulation results as saved in the output files. MIDA enables visualization of parameter posterior ~~probabilistic~~ density distributions with a Python script. In the script, MIDA first read accepted parameter values from "parameter_accepted.txt" file. Then, MIDA generates posterior probabilistic density function (PPDF) for each parameter via 'kdeplot' function in the 'seaborn' package. The maximum likelihood estimates of parameters correspond to the peaks of PPDF. The distinctive mode of PPDF indicates how well the parameter uncertainty is constrained. Finally, MIDA visualizes the PPDF for all parameters in a figure using the 'matplotlib' package.

2.6 Implementation and architecture of MIDA

MIDA is equipped with a graphical user interface (GUI) and users can easily execute it through an interactive window. Users can also run MIDA as a script program without the GUI. MIDA is

written in Python (version 3.7). For the GUI-version, all relevant Python packages used in MIDA are compiled together, thus users do not need to install them by themselves. For the non-GUI version, users need to install Python 3.7 and relevant packages (i.e., numpy, pandas, shutil, subprocess, matplotlib, math, os, and seaborn). MIDA is compatible with model source codes written in multiple programming language (e.g., Fortran, C/C++, C#, MATLAB, R, or Python). It is also independent of multiple operation systems (e.g., Windows, Linux, MacOS). In addition, MIDA is also able to run on high-performance computing (HPC) platforms via task management systems (e.g., Slurm).

The architecture of MIDA is class-based and each class is designed to describe an object (e.g., parameter, observations, etc.) with variables and operations. Five classes are defined in MIDA: parameter, observation, initialization, MCMC algorithm and the main program. The main program is the start of MIDA execution. It calls functions from all other classes to finish three-step workflow. As described in section 2.2, parameter and observation classes contain variables to be transferred in data exchanges via file I/O operations. These operations are implemented using the 'numpy' package. The initialization class is to read 'namelist.txt' in step 1 on data preparation and to assign values for the variables in all other classes. Then the class of MCMC algorithm conducts DA as described in step 2. In this step, the simulation operation uses a 'call' function in 'subprocess' package to call model executable. At the start of model simulation, MIDA writes new parameter values to the 'ParameterValue.txt' file in the 'working path' directory specified in step 1 on data preparation. Then the model executable read parameter values from the 'ParameterValue.txt' file and run. After model simulation, DA algorithm can read the model outputs by the output filenames indicated in the output configuration file. After DA, step 3 executes an additional Python script to read accepted parameter values and plot the

posterior density distributions of parameters. The plotting operations uses 'matplotlib' and 'seaborn' packages. The implementation of GUI uses pyQt5 toolkit to support interactive usage of MIDA. Users can also run MIDA in a non-interactive way with a 'main.py' script to trigger the three-step workflows.

2.7 User information of MIDA

In order to use MIDA, users need to prepare data and a model. The data to be used in MIDA are prior ranges and default values of parameters, parameter covariances, output configuration file, observations and their variances. They are organized in different files. Before running MIDA, users need to specify their filenames as suggested in step 1. When users want to use different data sets in DA, they can simply change filenames with the new data sets via GUI or in the 'namelist.txt' file. Figure C1 is an example of the 'namelist.txt' file for a data assimilation study with the DALEC model. The model to be used in MIDA should have those to-be-estimated parameter values not fixed in model source code rather than changeable through 'ParameterValue.txt' file. MIDA writes new parameter values in each proposing phase during DA to the 'ParameterValue.txt' file, from which the model reads the parameter values to run the simulation.

To calculate the cost function, J, we have to have a one-to-one match between observations and model outputs. For example, phenology models in one of the application cases of MIDA below generate discrete dates of leaf onset, which is a one-to-one match to the observations of spring leaf onset. In this case, observation $Z_i(t)$ and model output $X_i(t)$ to be used in calculation of J is straightforward. In the application case for dynamic vegetation, the data to be used are leaf area in six layers in a forest of 302 years old whereas the model simulates

leaf areas in eight layers from 0 to 800 years. To match observation, the model generates outputs of leaf areas in six layers when simulated forest age reaches 302 years. This requires users to prepare an output configuration file to instruct MIDA to read model outputs and re-organize their outputs to match observation. The output configuration file starts with a single line listing an observation filename and its corresponding output filenames. Content after the directories in the output configuration file are instructions to map model outputs with the observation signified in the first line. ~~Following lines are an instruction set to be operated on the output files signified above.~~ Each instruction is to match one or continuous elements in observation with elements in outputs with the same length. A blank line means there are no further instructions. Then a new matching between another observation and model outputs starts. An example of output configure file is available in Appendix B.

Once MIDA finishes the execution of data assimilation, users may need basic knowledge to assess the performance of DA. For example, the acceptance rate, which is given by MIDA, is the fraction of proposed parameter values that is accepted. Ideally, the acceptance rate should be about 230 ~ 540% (Xu et al., 2006). A very low acceptance rate indicates that many new proposed parameter values (CP_{new}) are rejected because CP_{new} jumps too far away from the previously accepted parameter values (Robert and Casella, 2013; Roberts et al., 1997). In this case, users are suggested to reduce a jump scale in the proposing phase. On the other hand, a very high acceptance rate is likely because CP_{new} moves slowly from the previously accepted parameter values. Users may increase the jump scale.

In addition, DA usually requires a convergence test to examine whether posterior distributions from different sampling series converge or not. Convergence test requires running DA parallelly or in multiple times with different initial parameter values. MIDA provides a

Gelman-Rubin (G-R) test (Gelman and Rubin, 1992) for this purpose. To use the G-R test, users need to prepare a file containing initial parameters values in different sampling series and indicate its filename in the 'namelist.txt' file as described in step 1. If the G-R statistics approaches one, the sampling series in DA is converged. When sampling series is converged, all accepted parameter values are used to generate the posterior distributions.

There are three types of posterior distributions: bell-shape, edge-hitting, and flat. The bell-shaped posterior distributions indicate that these parameters are well constrained. Their peak values are the maximum likelihood estimates of parameter values. The flat posterior distributions suggest that the parameters are not constrained due to the lack of relevant information in data. The edge-hitting posterior distributions result from complex reasons, such as improper prior parameter range. Users may change the prior ranges to examine if those posterior distributions can be improved or examine correlations among estimated parameters.

3. Applications of MIDA

We applied MIDA to four groups of models, which are an ecosystem carbon cycle model, a surrogate-based land surface model, nine phenology models, and a dynamic vegetation model, respectively. These four cases demonstrate that MIDA is effective for stand-alone DA, flexible to be applied to different models, and efficient for multiple model comparison.

3.1 Case 1: Independent data assimilation with DALEC

The first case study is to demonstrate that MIDA can be effective for independent data assimilation with the data assimilation linked ecosystem carbon (DALEC) model (Lu et al., 2017) ~~(Williams et al., 2005)~~. DALEC has been used for data assimilation in several studies (Bloom et al., 2016; Lu et al., 2017; Richardson et al., 2010; Safta et al., 2015; Williams et al.,

2005). Previous studies all incorporated data assimilation algorithms into DALEC, which requires invasive coding. This case study is focused on reproducing the data assimilation results as in the study by Lu et al. (2017) but with MIDA.

The version of DALEC used in this study is composed of six submodels (i.e., photosynthesis, phenology, autotrophic respiration, allocation, litterfall, and decomposition) to simulate the carbon exchanges among five carbon pools (i.e., leaf, stem, root, soil organic matter and litter) (Ricciuto et al., 2011). There are 21 parameters in DALEC, of which, 17 parameters are derived from the six submodels and four parameters serve to initialize the carbon pools. Table 2 summarizes the names, prior ranges and nominal values of these 21 parameters. The observation is the Harvard Forest daily net ecosystem exchange (NEE) from year 1992 to 2006. DALEC is coded in Fortran. In windows system, a gfortran compiler converts the model code to an executable file (i.e., DALEC.exe).

Figure 2 is the GUI window of MIDA. We first set up a DA task as described in step 1 using the upper panel. In this application, the number of sampling series is set as 20,000. Once users click the 'choose a directory' or 'choose a file' button, a new dialog window will pop up and users are able to choose the directory or load files interactively. As describe in step 1 on preparation of DA, the working path is where the outputs of DA and 'ParameterValue.txt' are saved (e.g., C:/workingPath). After the output configuration file is loaded, the filenames of model outputs, observations and their variance will be displayed in the window automatically. This application only uses a 'NEE.txt' observation file. Similarly, after users load parameter range file (e.g., a file named 'ParamRange.txt' contains three rows which are minimum, maximum and default values of parameters), the content in this file is displayed as well. To replace the current parameter range file loaded, users can simply upload another file. In this

application, the executive model file is 'DALEC.exe' with Fortran compiler in windows system. Because we do not have parameter covariance information, this input is left blank. After 'save to namelist file' is clicked, a 'namelist.txt' file containing all the inputs will be generated in the working path.

After the DA task set up, we load the 'namelist.txt' file and click the 'run data assimilation' button in the lower panel to trigger step 2 on execution of DA. A new dialog will pop up to show the acceptance rate information and notify the termination of DA. Then we will click the 'generate plots' button to visualize the posterior distributions of 21 parameters as described in step 3.

Figure 3 shows that the simulation outputs using the optimized parameter values from MIDA better fit with the observations than those using default parameter values. Figure 4 depicts posterior distributions of the 21 parameters estimated from MIDA. More than half of the parameters are constrained well with a unimodal shape. $X_{stem_{init}}$ and $X_{root_{init}}$ have a wide occupation of the prior range, indicating that the observation data does not provide useful information for them. The constrained posterior distributions in this study are similar to those from the study in Lu et al. (2017). Note that MCMC estimates have a large variance and a low convergence rate especially in high-dimensional problems, with a finite number of samples it is not expected that two simulations would give exactly the same results.

3.2 Case 2: Application of MIDA to a surrogate land surface model

This case study is to examine the applicability of MIDA to a surrogate-based land surface model. The original model is energy exascale earth system model: the land component (ELM) (Ricciuto et al., 2018). As ELM is computationally expensive (one forward model simulation takes more than one day), a sparse-grid (SG) surrogate system was developed to reduce the computational

time (Lu et al., 2018). The forcing data for the surrogate model is half-hourly meteorological measurements at Missouri Ozark flux site from 2006 to 2014. The observations that were used for optimization are annual sums of net ecosystem exchange (NEE), annual averages of total leaf area index and latent heat fluxes from 2006 to 2010. The eight parameters selected (Table 3) are the most important parameters for the variations in outputs (Ricciuto et al., 2018). The model is written in Python. A 'pyinstaller' library packages the model code into an executable file. The iteration number in MIDA is 20,000.

Figure 5 shows posterior distributions of calibrated parameters. c_{root}, SLA_{top}, $t_{leaffall}$, GDD_{onset} are constrained well with a unimodal distribution. However, the distribution of the rest 4 parameters (i.e., N_{leaf}, CN_{root}, A_{r2l} and Res_m) cluster at near the edge. These results match well with the study by Lu et al. (2018). As shown in Figure 6, the calibrated parameters induce a performance improvement in simulating total leaf area index and NEE. For latent heat, both the default and optimized simulation obtain good agreement with the observation. These conclusions are also similar to those in Lu et al. (2018).

MIDA hides the detailed differences between models. For example, DALEC model in case 1 is a process-based model to simulate ecosystem carbon cycle while surrogate-based ELM in case 2 is an approximation of land surface model. They are also different in programming language, simulation time, forcing data, etc. MIDA is able to deal with models with so many different characteristics and hides these differences from users. Users only need to indicate the filenames of the model to be used, its parameter range, the output configuration file, etc. in the 'namelist.txt' file. Thus, MIDA simplified the DA applications using different models.

3.3 Case 3: Evaluation of multiple phenological models

This study case uses nine phenological models (Yun et al., 2017) to demonstrate the applicability of MIDA in model comparison. Five out of the nine models predict phenological events, such as the day of leaf onset, using growing degree days, which are calculated as temperature accumulation above a base temperature. The other four models consider two processes: chilling effects of cold temperature on dormancy before budburst and forcing effects of warm temperature on plant development. Each model uses different response functions to represent chilling and forcing effects. The detailed model descriptions and associated parameter information are in supplementary table.

Data are from the Spruce and Peatland Responses Under Climatic and Environmental Change experiment (SPRUCE) (Hanson et al., 2017) located in northern Minnesota, USA. The experiment consists of five-level whole-ecosystem warming (i.e., +0, +2.25, +4.5, +6.75, +9°C) and two-level elevated CO_2 concentrations (i.e., +0, +500ppm). Dates of leaf onset were observed with PhenoCam (Richardson et al., 2018) for tree species: *Picea mariana* and *Larix laricina*. For the sake of demonstration of MIDA application, we only show DA results for *Larix laricina* with +9°C warming treatment and +0 ppm CO_2 treatment from 2016 to 2018.

MIDA was used to compare performances of the nine models in reference to the same observations of leaf onset dates after DA. We as users changed filenames of model executable file (i.e., PhenoModels.exe), defined parameter ranges, and assigned the directory of working path for each model. MIDA then estimated the optimized parameters and save the corresponding best simulation outputs to the working path for each of the nine models. Figure 7 shows the best simulation output of these nine models. The simulation output of the 6^{th}, 7^{th}, 8^{th}, and 9^{th} models better fit the observation than the other models. It demonstrates that models that consider both chilling and heating effects can achieve good simulations of the leaf onset dates.

3.4 Case 4: Supporting data assimilation with a dynamic vegetation model

This case study is to examine the efficiency of MIDA to integrate remote sensing data into a dynamic vegetation model. The model used in this study is Biome Ecological strategy simulator (BiomeE) (Weng et al., 2019). This model ~~is to~~ simulate~~s~~ vegetation demographic processes with individual-based competition for light, soil water, and nutrients. Individual trees in BiomeE model are represented by cohorts of trees with similar sizes. The light competition among cohorts is based on their heights and crown areas according to the rule of perfect plasticity approximation (PPA) model (Strigul et al., 2008). Each cohort has seven pools: leaves, roots, sapwood, heartwood, seeds, nonstructural carbon and nitrogen. After carbon are assimilated into plants via photosynthesis, the assimilated carbon enters to nonstructural carbon pool and is used for plant growth (i.e., diameter, height, crown area) and reproduction according to empirical allomeric equations (Weng et al., 2019). In this application, two parameters to be constrained (Table 4) are annual productivity rate and annual mortality rate of trees.

Observations to be used in DA are leaf area indexes in six vertical heights (i.e., 0-5m, 6-10m, 11-15m, 16-20m, 21-25m, and 26-30m) at Willow Creek study site, Wisconsin, USA. The forest at the site is an upland deciduous broadleaf forest of around 302 years old. The observations were from Global Ecosystem Dynamics Investigation (GEDI) acquired by a Light Detection and Ranging (Lidar) laser system, which is deployed on the International Space Station (ISS) by NASA in 2018 (Dubayah et al., 2020). The observations were first averaged from three footprints and then leaf area indexes in the six canopy layers were standardized to be summed up as one.

To use MIDA, we reorganized the simulation outputs to match observations as suggested in section 2.6. The BiomeE model simulates leaf areas in eight layers (i.e., 0-5m, 6-10m, 11-15m, 16-20m, 21-25m, 26-30m, 31-35m, and 36-40m) from 0 to 800 years. An output configuration file was provided to post-process model outputs of leaf area indexes in six layers to match observations at the forest age of 302 years. These simulated leaf area indexes in the six canopy layers were also standardized to match standardized observations of leaf area indexes. The observations and post-processed simulation outputs were saved to 'LAI.txt' and 'simu_LAI.txt' files, respectively. The two files are used in MIDA for data assimilation to generate posterior distributions of estimated two parameters as showed in figure 8. The optimized parameter values through maximum likelihood estimation are different from their default values. Figure 9 compares the simulation outputs with optimized parameters estimated by MIDA to those with default parameter values. After DA with GEDI data in MIDA, the simulation accuracy of leaf area index is substantially improved especially in middle (16~20m) and highest (26~30m) layers.

4. Discussion

This study introduced MIDA as a model-independent tool to facilitate the applications of data assimilation in ecology and biogeochemistry. The potential user community is ecologists with limited knowledge of model programming and technical implementation of DA algorithms. Several model-independent DA tools have already been developed, such as DART (Anderson et al., 2009), openDA (Ridler et al., 2014), PDAF (Nerger and Hiller, 2013) and PEST (Doherty, 2004), mainly for applications in research areas of hydrology, atmosphere, and remote sensing. These DA tools either use gradient descent method, such as Levenburg-Marqurdt algorithm in

PEST, or Kalman Filter methods, such as EnKF in DART, openDA, and PDAF. The Levenburg-Marqurdt algorithm is a local search method, which is hard to find global optimization solution for highly nonlinear models. EnKF updates state variables and parameter values each time when observations are sequentially assimilated, resulting discrete values of estimated parameters. Jumps in estimated parameter values by EnKF make it very difficult to obey mass conservation in biogeochemical models (Gao et al., 2011). In this study, we used the MCMC method in MIDA to generate~~s~~ parameter values and their posterior distributions. MCMC is a widely used method in many DA studies with biogeochemical models but has been applied to individual models with invasive coding (Bloom et al., 2016; Hararuk et al., 2015; Liang et al., 2018; Luo and Schuur, 2020; Ricciuto et al., 2011). Compared to the other model-independent DA tools mentioned above, MIDA is the first tool that uses the MCMC method for DA.~~MIDA is the first model-independent tool that uses the MCMC method for DA.~~

Biogeochemical models are incorporating more detailed processes related to carbon and nitrogen cycles (Lawrence et al. 2020). Complex biogeochemical models yield predictions with great uncertainty (Frienlingstein et al. 2009 and 2014). Data assimilation has been increasingly used to estimate parameter values against observations and reduce uncertainty in model prediction (Luo et al. 2016, Luo and Schuur 2020). However, current applications of DA are almost all model dependent. It requires ecologists to write code to integrate DA algorithm with models. The coding practice is a big technical challenge for ecologists with limited program ability. The distinct advantage of MIDA is to enable ecologists to conduct model independent DA. MIDA streamlines workflow of the three-step procedure for DA to enable users to conduct DA without extensive coding. Users mainly need to provide numerical and character values for data exchanges to transfer data (i.e., parameter values, simulation outputs, observations) between

the model and MIDA by a file named ‘namelist.txt’ or by interactive inputs via a GUI window (Fig. ~~1~~2).

We tested MIDA in four cases for its applicability to ecological models. The first case is applied to DALEC model, which has been used in several data assimilation studies (Bloom et al., 2016; Lu et al., 2017; Safta et al., 2015; Williams et al., 2005). The previous DA studies all used invasive coding to incorporate DA algorithm into models. As demonstrated in this study, MIDA was applied to DALEC without invasive coding but by providing the directory to save DA results and filenames of DALEC model executable, parameter prior range, and output configuration file through the ‘namelist.txt’ file or interactive inputs in the first preparation step of the workflow. Then, MIDA run DA as a black box with DALEC before visualizing the DA results. Next, we tested the applicability of MIDA a surrogate-based ELM model and a dynamic vegetation model BiomeE. To switch the test case from DALEC to the surrogate-based ELM model and the BiomeE model, we changed the filenames of model executable, parameter prior range, and output configuration file in the ‘namelist.txt’ file for MIDA. This flexibility of MIDA in switching models for DA makes it much easier for model comparisons. We tested this capability of MIDA with nine phenological models to compare alternative model structures. Similarly, MIDA enables efficient switches of observations to be assimilated into models. Users only need to change filenames of observations in the output configuration file. This feature of MIDA makes it easier to utilize abundant traits databases such as TRY (Kattge et al., 2020), FRED (Iversen et al., 2017), etc. Moreover, this feature of MIDA also helps evaluating the relative information content of different observations for constraining model parameters and prediction (Weng and Luo, 2011). Consequently, MIDA can facilitate selection of the most informative observations and then better guide data collections in filed experiments. Ultimately,

MIDA can aid ecological forecasting and help reduce uncertainty in model predictions (Huang et al., 2018; Jiang et al., 2018).

Although MIDA helps users to get rid of model detail, users may still need basic knowledge about the model outputs to prepare the output configuration file which is to match model outputs to observations one-by-one (see Section 2.6). This effort of preparing the correspondence between model outputs and observations for MIDA is not that difficult because users are reading or writing a text file and most model developers will provide reference to help understanding observations or model output files.

Generally, MIDA requires longer time to run DA than the embedded DA algorithm, because MIDA calls model simulation as an external executable rather than a function embedded. Thus, we recommend MIDA for beginners of DA users with models that are less complex. Besides, t~~T~~he current version of MIDA only incorporates Metropolis-Hasting sampling approach. More MCMC methods (e.g., Hamiltonian Monte Carlo) may be incorporated into MIDA in the future.

5. Conclusions

We developed MIDA to facilitate data assimilation for biogeochemical models. Traditional DA studies require ecologists to program codes to integrate DA algorithms into model source codes. The easy-to-use MIDA module enables ecologists to conduct model-independent DA without extensive coding thus advancing the application of DA for ecological modeling and forecasting. We demonstrated the capability of MIDA in four cases with a total of 12 ecological models. These cases showed that MIDA is easy to perform for a variety of models and can efficiently produce accurate parameter posterior distributions. Moreover, MIDA supports flexible usage of

596 different models and different observations in the DA analysis and allows a quick switch from
597 one model to another. This capability enables MIDA to serve as an efficient tool for model
598 intercomparison projects and enhancing ecological forecasting.
599
600 **Appendix A:** Nine phenological models
601 1. Growing degree (GD)
602 The growing degree (GD) model is one of the most widespread phenological model to simulate
603 the date of leaf onset ($\widehat{D}$). In this study, the time scale is limited to daily based on observation
604 records. The kernel of GD is to calculate the growing degree days (GDD, $\sum_{d=D_s}^{\widehat{D}-1}\Delta d$) which is the
605 heat accumulation above a base temperature (T_b). For simplicity, the daily temperature (T_d) can
606 be approximated by the average of daily maximum and minimum temperatures. The heat
607 accumulation starts at day D_s, which is empirically estimated, and ends when GDD reaches a
608 forcing requirement threshold (R_d). Two parameters to be constrained are base temperature (T_b)
609 and the forcing requirement (R_d). Their default values and prior range are listed in Table A1.

610 $$\Delta d = \begin{cases} T_d - T_b \; if \; T_d > T_b \\ 0 \quad otherwise \end{cases} \quad \text{(A1)}$$

611 $$\sum_{d=D_s}^{\widehat{D}-1}\Delta d < R_d \leq \sum_{d=D_s}^{\widehat{D}}\Delta d \quad \text{(A2)}$$

612 2. Sigmoid function (SF)
613 Compared to the linear response function of GDD in GD model, the sigmoid function (SF)
614 model provides a non-linear function to better represent the non-linearity of the growth response
615 to heat accumulation. Three parameters to be constrained in DA are base temperature (T_b), the
616 forcing requirement (R_d) and temperature sensitivity (S_t). Their default values and prior range
617 are listed in Table A1.

Formatted: Font: 12 pt
Formatted: Font: 12 pt
Formatted: Font: 12 pt
Formatted: Font: 12 pt
Formatted: Font: 12 pt
Formatted: Right
Formatted: Font: 12 pt
Formatted: Font: 12 pt
Formatted: Font: 12 pt
Formatted: Font: 12 pt
Formatted: Font: 12 pt
Formatted: Font: 12 pt
Formatted: Font: 12 pt
Formatted: Font: 12 pt
Formatted: Font: 12 pt
Formatted: Font: 12 pt
Formatted: Font: 12 pt
Formatted: Font: 12 pt
Formatted: Font: 12 pt
Formatted: Font: 12 pt
Formatted: Font: 12 pt
Formatted: Font: 12 pt
Formatted: Font: 12 pt
Formatted: Font: 12 pt
Formatted: Font: 12 pt
Formatted: Font: 12 pt
Formatted: Font: 12 pt
Formatted: Font: 12 pt
Formatted: Font: 12 pt
Formatted: Font: 12 pt
Formatted: Font: 12 pt
Formatted: Font: 12 pt
Formatted: Font: 12 pt
Formatted: Font: 12 pt
Formatted: Font: 12 pt

$$\Delta d = \frac{1}{1+e^{S_f(T_d - T_b)}} \quad \text{(A3)}$$

$$\sum_{d=D_s}^{\tilde{D}-1} \Delta d < R_d \leq \sum_{d=D_s}^{\tilde{D}} \Delta d \quad \text{(A4)}$$

3. Beta function (BF)

In reality, the plant growth rate, as described with Δd, gradually increases up to a specific temperature, then rapidly declines to a supra-optimal level. Such response can be well described by a beta function with uni-modality and non-symmetrical shape. Three parameters are involved in DA: minimum temperature (T_n), optimal temperature (T_o) and forcing requirement (R_d). The other parameter values are fixed with empirical values. For example, maximum growth rate (R_x) is set to one and maximum temperature (T_x) is assumed to be 45.

$$r_d = R_x \left(\frac{T_x - T_d}{T_x - T_o}\right)\left(\frac{T_d - T_n}{T_o - T_n}\right)^{\frac{T_o - T_n}{T_x - T_o}} \quad \text{(A5)}$$

$$\Delta d = \begin{cases} r_d \ \ if\ r_d > 0 \\ 0 \ otherwise \end{cases} \quad \text{(A6)}$$

$$\sum_{d=D_s}^{\tilde{D}-1} \Delta d < R_d \leq \sum_{d=D_s}^{\tilde{D}} \Delta d \quad \text{(A7)}$$

4. Days transferred to standard temperature (DTS)

According to Arrhenius las, the relationship between growth rate and daily temperature T_d can be interpolated by the equation 8 (Ono and Konno, 1999). With a factor weighted by standard temperature, the equation for DTS (Eq. A9) can better represent growth rate dependent on temperatures. Three parameters considered in DA are: temperature sensitivity rate (E_a), standard temperature (T_s) and forcing requirement (R_d).

$$k = e^{\frac{-E_a}{R \cdot T_d}} \quad \text{(A8)}$$

$$\Delta d = e^{\frac{E_a (T_d - T_s)}{R \cdot T_d \cdot T_s}} \quad \text{(A9)}$$

$$\sum_{d=D_s}^{\tilde{D}-1} \Delta d < R_d \leq \sum_{d=D_s}^{\tilde{D}} \Delta d \quad \text{(A10)}$$

Formatted: Font: 12 pt
Formatted: Right
Formatted ...
Formatted: Font: 12 pt
Formatted: Right
Formatted ...
Formatted ...
Formatted ...
Formatted: Font: 12 pt
Formatted: Right
Formatted ...
Formatted ...
Formatted ...

5. Thermal period fixed model (TP)

The difference between GD and TP models are heat accumulation occurs in a fixed time period (D_n). The day of leaf onset is the last day ($\widehat{D_s} + D_n$) when the accumulated heat reaches the forcing requirement. The start day ($\widehat{D_s}$) of heat accumulation begins in day one and moves one day forward each time to estimate Eq. (A12). Three parameters are involved in DA: the base temperature (T_b), the period length (D_n) and the forcing requirement (R_d).

$$\Delta d = \begin{cases} T_d - T_b \ if \ T_d > T_b \\ 0 \quad otherwise \end{cases} \quad \text{(A11)}$$

$$R_d \leq \sum_{d=\widehat{D_s}}^{\widehat{D_s}+D_n} \Delta d \quad \text{(A12)}$$

6. Chilling and forcing (CF)

Compared to GD, there is another distinctive chilling period for dormancy. CF model sequentially calculates two accumulations in opposite directions: chilling accumulation and anti-chilling accumulation. The start day of chilling accumulation (D_s) is implicitly set as 273.0 which is October 1st. The end day of chilling accumulation (D_0) is the beginning of anti-chilling accumulation. Three parameters are considered in DA: the chilling requirement (R_d^C) and the forcing requirement (R_d^F), the temperature threshold (T_c).

$$\Delta d = \begin{cases} T_d - T_c \ if \ T_d \geq 0 \\ -T_a \quad otherwise \end{cases} \quad \text{(A13)}$$

$$\Delta_d^C = \begin{cases} \Delta d \ if \ \Delta d < 0 \\ 0 \ otherwise \end{cases} \quad \text{(A14)}$$

$$\Delta_d^F = \begin{cases} \Delta d \ if \ \Delta d > 0 \\ 0 \ otherwise \end{cases} \quad \text{(A15)}$$

$$\sum_{d=D_s}^{D_0-1} \Delta_d^C > R_d^C \geq \sum_{d=D_s}^{D_0} \Delta_d^C \quad \text{(A16)}$$

$$\sum_{d=D_0}^{\widehat{D}-1} \Delta_d^F < R_d^F \leq \sum_{d=D_0}^{\widehat{D}} \Delta_d^F \quad \text{(A17)}$$

7. Sequential model (SM)

The difference between CF and SM models is that SM used a beta function (Eq. A18) for the calculation of chilling accumulation and adopted a sigmoid function (Eq. A20) for anti-chilling accumulation. The detailed descriptions of these two functions can be referred to the introductions of BF model and CF model. The maximum temperature is empirically set as 13.7695. Six parameters are constrained in DA: minimum temperature (T_n), optimal temperature (T_o), temperature sensitivity (S_t), forcing base temperature (T_b), chilling requirement (R_d^C), and forcing requirement (R_d^F).

$$r_d = \left(\frac{T_x - T_d}{T_x - T_o}\right)\left(\frac{T_d - T_n}{T_o - T_n}\right)^{\frac{T_o - T_n}{T_x - T_o}} \quad \text{(A18)}$$

$$\Delta_d^C = \begin{cases} r_d \ \ if\ r_d < 0 \\ 0 \ otherwise \end{cases} \quad \text{(A19)}$$

$$\Delta_d^F = \frac{1}{1 + e^{S_t(T_d - T_b)}} \quad \text{(A20)}$$

$$\sum_{d=D_s}^{D_0 - 1} \Delta_d^C > R_d^C \geq \sum_{d=D_s}^{D_0} \Delta_d^C \quad \text{(A21)}$$

$$\sum_{d=D_0}^{\bar{D} - 1} \Delta_d^F < R_d^F \leq \sum_{d=D_0}^{\bar{D}} \Delta_d^F \quad \text{(A22)}$$

8. Parallel model (PM)

Critical difference between PM and above two-step models is that the chilling and anti-chilling accumulations happen simultaneously (Fu et al., 2012). In the earlier dates during chilling period, only small fraction (K_d) of forcing (Eq. A25) will be accumulated. The maximum temperature is empirically set as 15.3. Seven parameters will be considered in DA: minimum temperature (T_n), optimal temperature (T_o), temperature sensitivity (S_t), forcing base temperature (T_b), chilling requirement (R_d^C), forcing requirement (R_d^F), and a forcing weight coefficient (K_m).

$$r_d = \left(\frac{T_x - T_d}{T_x - T_o}\right)\left(\frac{T_d - T_n}{T_o - T_n}\right)^{\frac{T_o - T_n}{T_x - T_o}} \quad \text{(A23)}$$

$$\Delta_d^C = \begin{cases} r_d \ \ if\ r_d < 0 \\ 0 \ otherwise \end{cases} \quad \text{(A24)}$$

Formatted ...
Formatted: Right
Formatted ...
Formatted ...
Formatted ...
Formatted ...
Formatted ...
Formatted: Right
Formatted ...

$$K_d = \begin{cases} K_m + (1 - K_m)\frac{\sum_{i=D_s}^{d} \Delta_i^C}{R_d^C} & if \ \sum_{d=D_s}^{D_0-1} \Delta_d^C > R_d^C \\ 1 & otherwise \end{cases} \quad \text{(A25)}$$

$$\Delta_d^F = \frac{K_d}{1+e^{St(T_d - T_b)}} \quad \text{(A26)}$$

$$\sum_{d=D_s}^{D_0-1} \Delta_d^C > R_d^C \geq \sum_{d=D_s}^{D_0} \Delta_d^C \quad \text{(A27)}$$

$$\sum_{d=D_0}^{\bar{D}-1} \Delta_d^F < R_d^F \leq \sum_{d=D_0}^{\bar{D}} \Delta_d^F \quad \text{(A28)}$$

9. Alternating model (AM)

AM fixes the start date of chilling period (D_s^C) as November 1st and the start date of anti-chilling period (D_s^F) as January 1st. The difference between AM and the other models above is that the forcing requirement is not a parameter value but is decided by the length of chilling days (Fu et al., 2012). Five parameters to be constrained in DA are: chilling temperature (T_c), forcing base temperature (T_b) and three coefficients (a, b, c) in calculation of forcing requirement.

$$\Delta_d^C = \begin{cases} 1 \ if \ T_d \leq T_c \\ 0 otherwise \end{cases} \ \text{~~(A29)~~} \quad \text{(A29)}$$

$$\Delta_d^F = \begin{cases} T_d - T_b \ if \ T_d > T_b \\ 0 \quad otherwise \end{cases} \ \text{~~(A30)~~} \quad \text{(A30)}$$

$$R_d^C = \sum_{i=D_s^C}^{d} \Delta_i^C \ \text{~~(A31)~~} \quad \text{(A31)}$$

$$R_d^F = a + b \cdot e^{-c \cdot R_d^C} \ \text{~~(A32)~~} \quad \text{(A32)}$$

$$\sum_{d=D_s^F}^{\bar{D}-1} \Delta_d^F < R_d^F \leq \sum_{d=D_s^F}^{\bar{D}} \Delta_d^F \ \text{~~(A33)~~} \quad \text{(A33)}$$

Formatted ...

Formatted ...

Formatted ...

Formatted: Right

Formatted ...

Formatted ...

Formatted ...

Formatted ...

Formatted ...

Table A1: A summary of parameters to be calibrated in nine phenological models. Their default parameter value and prior parameter range are shown.

Model	Parameter	Description	Unit	Default	Range
GD	T_b	Base temperature	℃	10	[-5, 25]
	R_d	Forcing requirement	℃d	35	[0, 200]
SF	T_b	Base temperature	℃	-1.5	[-10, 25]
	R_d	Forcing requirement	℃	50	[0, 500]
BF	T_o	Optimal temperature	℃	15	[10, 35]
	T_n	Minimum temperature	℃	0	[-10, 5]
	R_d	Forcing requirement	℃d	11	[0, 50]
DTS	E_a	Temperature sensitivity rate	-	250	[1, 1500]
	T_s	Standard temperature	℃	10	[-30, 40]
	R_d	Forcing requirement	℃d	50	[1, 200]
TP	T_b	Base temperature	℃	12.5	[0, 30]
	D_n	Period length	d	25	[0, 50]
	R_d	Forcing requirement	℃d	20	[0, 150]
CF	R_d^C	Chilling requirement	℃d	-124	[-300, 0]
	R_d^F	Forcing requirement	℃d	120	[0, 300]
	T_c	Chilling base temperature	℃	5	[0, 30]
SM	T_n	Minimum temperature	℃	-20	[-80, 0]
	T_o	Optimal temperature	℃	0	[-26, 10]
	S_t	Temperature sensitivity	-	-1.8	[-5, 0]
	T_b	Forcing base temperature	℃	5	[-5, 35]
	R_d^C	Chilling requirement	℃d	20	[0, 80]
	R_d^F	Forcing requirement	℃d	20	[0, 80]
PM	T_n	Minimum temperature	℃	-20	[-80, 0]
	T_o	Optimal temperature	℃	0	[-26, 10]
	S_t	Temperature sensitivity	-	-0.6	[-1, 0]
	T_b	Forcing base temperature	℃	5	[-5, 35]
	R_d^C	Chilling requirement	℃d	11.35	[0, 80]
	R_d^F	Forcing requirement	℃d	44.01	[0, 80]
	K_m	Forcing weight coefficient	-	0.2	[0, 1]
AM	T_c	Chilling base temperature	℃	4.6	[-10, 10]
	T_b	Forcing base temperature	℃	5	[-5, 35]
	a	Coefficient for forcing adjustment	-	11.51	[0.01, 15]
	b	Coefficient for forcing adjustment	-	88	[0, 200]
	c	Coefficient for forcing adjustment	-	-0.01	[-1, -10^{-4}]

Appendix B: An example of output configuration file

Output configuration file (e.g., config.txt) is to indicate the directories of observations and ~~their models~~simulation output files as well as how they map to each other. Figure B1 is an example of the output configuration file. There are three blocks of functions to map simulation outputs to observed GPP, RE, and NEE. The blocks of mapping functions are separated by a blank line. Each mapping block starts with the directories of one observation, its observation variance and model outputs, which are separated by a hash key. If there is no observation variance available, users can ignore this directory. If multiple simulation outputs are used to correspond to one observation, the directories of simulation outputs are separated by a comma. The rest of the mapping block describes how to map simulation outputs to observations. The simu_map variable is simulation output after mapping. The simuList variable saves the simulation outputs specified in the first line. Taking the third mapping block in Fig. B1 as an example, simuList[0] saves contents in simuNEE_1.txt and simuList[0][0:365] saves the first 365 elements in this file.

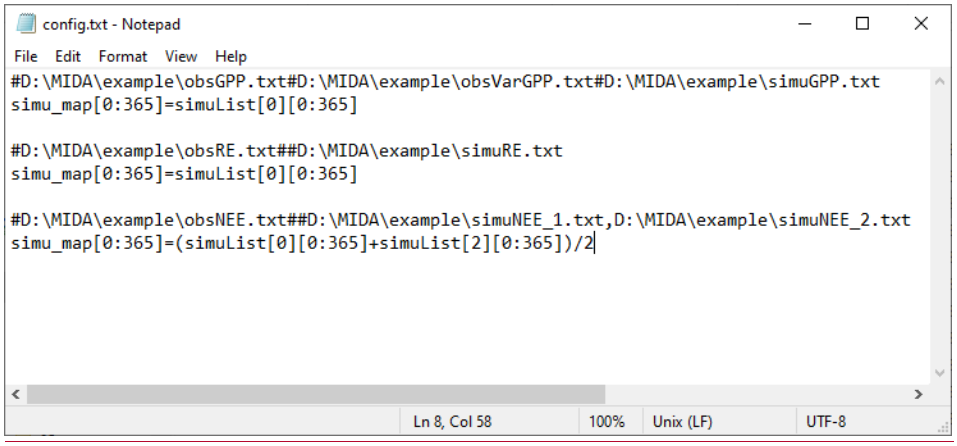

Figure B1: An example of output configuration file

Formatted: Level 1, Space After: 0 pt, Line spacing: Double

Formatted: Font: Not Bold

Appendix C: An example of the namelist.txt file

The Fig. C1 shows an example of the namelist.txt for the first study case with the DALEC model. Users need to prepare the namelist.txt before execution of data assimilation (DA) either manually or via GUI. Below describes the content in the namelist.txt. Detailed explanation or tutorials are available in the Zenodo repositories at the end of the appendixes.

'workpath' is the directory where the MIDA executable are saved. 'nsimu' is the number of iterations in execution of data assimilation. 'J_default' is the default mismatch (i.e., cost function) to be compared in the first moving phase of data assimilation. 'ProposingStepSize' controls the jump scale in the proposing phase of data assimilation. Users can increase or decrease this value to adjust the acceptance rate to be in a range from 0.2 to 0.5. 'paramFile' is the directory of a csv file saving parameter-related information such as parameter range. 'obsList' saves the directories of observations. Multiple observations are separated by semicolon. Similarly, 'obsVarList' saves the directories of observation variance in the same order as that of 'obsList'. 'simuList' saves the directories of simulation outputs corresponding to the observations. With GUI, MIDA reads directories in the output configuration file (e.g., config.txt) which users provide and assign values for 'obsList','obsVarList', and 'simuList' in the namelist.txt automatically. In this case, if the directories of observations change, users only need to modify the output configuration file and generate the namelist.txt again with GUI-based MIDA.

'paramValue' is the directory of a txt file where MIDA writes out new set of parameter values for model execution in each iteration of data assimilation. Its default value is 'ParameterValue.txt' under the workpath specified in the first line of the namelist.txt. 'model' saves the directory of model executable. 'nChains_convergeTest' indicates whether to conduct

German-Rubin (G-R) convergence test or not. If G-R test is used, its values is the number of multiple MCMC chains. If not, its value is zero. 'convergeTest_startsFile' is the directory of a ~~txt~~csv file saving default parameter values as the start points in multiple MCMC chains. 'outConvergenceTest' saves the results of G-R test. If 'nChains_ConvergeTest' is zero, both values of 'convergeTest_startsFile' and 'outConvergenceTest' are empty. 'DAresultsPath' is the directory saving the results of DA whose directories are also listed in the following six lines: 'outJ' for the accepted mismatches; 'outC' for the accepted parameter values; 'outRecordNum' for the number of accepted parameter values; 'outBestSimu' for the best simulation outputs with the optimal parameter values; 'outBestC' for the optimal parameter values. For MIDA without GUI, 'display_plot' indicates whether or not to visualize the posterior distributions after DA.

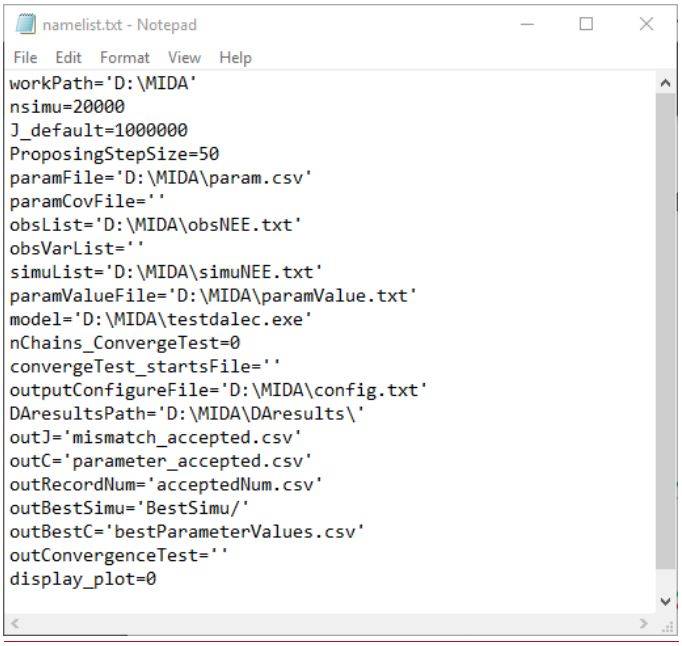

Figure C1. An example of the 'namelist.txt' file. In order to use MIDA, users need to prepare data and a model and specify their file names and directories in the 'namelist.txt' file.

Code and data availability. The code of MIDA is available at the Zenodo repository https://doi.org/10.5281/zenodo.4762725 (last access: May 2021). Data used in this study are available at https://doi.org/10.5281/zenodo.4762779. A comparison of the time cost using the embedded DA algorithm and MIDA is available at the Zenodo repository https://doi.org/10.5281/zenodo.4891319.

Video supplement. Tutorial videos of how to use MIDA is available at https://doi.org/10.5281/zenodo.4762777

~~*Code and data availability*. The code of MIDA is available at the GitHub repository https://github.com/Celeste-Huang/MIDA (last access: Feb 2021). Data used in this study are available at https://github.com/Celeste-Huang/MIDA/tree/main/Example.~~

~~*Video supplement*. A tutorial video of how to use MIDA is available at https://github.com/Celeste-Huang/MIDA/tree/main/Videos~~

Author contributions. XH, IS, and YL designed the study. XH built the workflow of MIDA and tested its capability in four cases. DL, DMR, and PJH provided data and model for the first and second test cases. XL prepared models and ADR provided observations for the third case. EW and SN helped to prepare data and model for the fourth case. XH, LJ, EH and YL analyzed the results. All authors contributed to the preparation of the manuscript.

Competing interests. The authors declare that they have no conflict of interest.

Acknowledgements. This work was funded by subcontract 4000158404 from Oak Ridge National Laboratory (ORNL) to the Northern Arizona University. ORNL is managed by UT-Battelle, LLC, for the U.S. Department of Energy under contract DE-AC05-00OR22725.

References

Allen, J. I., Eknes, M. and Evensen, G.: An Ensemble Kalman Filter with a complex marine ecosystem model: hindcasting phytoplankton in the Cretan Sea, Ann. Geophys., 21(1), 399–411, doi:10.5194/angeo-21-399-2003, 2003.

Anderson, J., Hoar, T., Raeder, K., Liu, H., Collins, N., Torn, R. and Avellano, A.: The data assimilation research testbed a community facility, Bull. Am. Meteorol. Soc., 90(9), 1283–1296, doi:10.1175/2009BAMS2618.1, 2009.

Bloom, A. A., Exbrayat, J. F., Van Der Velde, I. R., Feng, L. and Williams, M.: The decadal state of the terrestrial carbon cycle: Global retrievals of terrestrial carbon allocation, pools, and residence times, Proc. Natl. Acad. Sci., 113(5), 1285–1290, doi:10.1073/pnas.1515160113, 2016.

Bonan, G.: Climate Change and Terrestrial Ecosystem Modeling, Cambridge University Press., 2019.

Box, G. E. P. and Tiao, G. C.: Bayesian Inference in Statistical Analysis, John Wiley & Sons, Inc., Hoboken, NJ, USA., 1992.

Ciais, P., Chris, S., Govindasamy, B., Bopp, L., Brovkin, V., Canadell, J., Chhabra, A., Defries, R., Galloway, J. and Heimann, M.: Carbon and other biogeochemical cycles, Clim. Chang. 2013 Phys. Sci. Basis, 465–570, 2013.

Cline, M. P., Lomow, G. and Girou, M.: C++ FAQs, Pearson Education., 1998.

Formatted: Indent: Hanging: 0.2"

798 Doherty, J.: PEST: Model independent parameter estimation. Fifth edition of user manual,
799 Watermark Numer. Comput., doi:10.1016/B978-0-08-098288-5.00031-2, 2004.
800 Evensen, G.: The Ensemble Kalman Filter: Theoretical formulation and practical implementation,
801 Ocean Dyn., 53(4), 343–367, doi:10.1007/s10236-003-0036-9, 2003.
802 Fer, I., Kelly, R., Moorcroft, P. R., Richardson, A. D., Cowdery, E. M. and Dietze, M. C.: Linking
803 big models to big data: Efficient ecosystem model calibration through Bayesian model
804 emulation, Biogeosciences, 15(19), 5801–5830, doi:10.5194/bg-15-5801-2018, 2018.
805 Fox, A., Williams, M., Richardson, A. D., Cameron, D., Gove, J. H., Quaife, T., Ricciuto, D.,
806 Reichstein, M., Tomelleri, E., Trudinger, C. M. and Van Wijk, M. T.: The REFLEX project:
807 Comparing different algorithms and implementations for the inversion of a terrestrial ecosystem
808 model against eddy covariance data, Agric. For. Meteorol., 149(10), 1597–1615,
809 doi:10.1016/j.agrformet.2009.05.002, 2009.
810 Fox, A. M., Hoar, T. J., Anderson, J. L., Arellano, A. F., Smith, W. K., Litvak, M. E., MacBean, N.,
811 Schimel, D. S. and Moore, D. J. P.: Evaluation of a Data Assimilation System for Land Surface
812 Models Using CLM4.5, J. Adv. Model. Earth Syst., 10(10), 2471–2494,
813 doi:10.1029/2018MS001362, 2018.
814 Friedlingstein, P., Cox, P., Betts, R., Bopp, L., von Bloh, W., Brovkin, V., Cadule, P., Doney, S.,
815 Eby, M., Fung, I., Bala, G., John, J., Jones, C., Joos, F., Kato, T., Kawamiya, M., Knorr, W.,
816 Lindsay, K., Matthews, H. D., Raddatz, T., Rayner, P., Reick, C., Roeckner, E., Schnitzler, K.-
817 G., Schnur, R., Strassmann, K., Weaver, A. J., Yoshikawa, C. and Zeng, N.: Climate–Carbon
818 Cycle Feedback Analysis: Results from the C4MIP Model Intercomparison, J. Clim., 19(14),
819 3337–3353, doi:10.1175/JCLI3800.1, 2006.
820 Fu, Y. H., Campioli, M., Van Oijen, M., Deckmyn, G. and Janssens, I. A.: Bayesian comparison of

821 six different temperature-based budburst models for four temperate tree species, Ecol. Modell.,
822 230, 92–100, doi:10.1016/j.ecolmodel.2012.01.010, 2012.
823 Gao, C., Wang, H., Weng, E., Lakshmivarahan, S., Zhang, Y. and Luo, Y.: Assimilation of multiple
824 data sets with the ensemble Kalman filter to improve forecasts of forest carbon dynamics, Ecol.
825 Appl., 21(5), 1461–1473, doi:10.1890/09-1234.1, 2011.
826 Gelman, A. and Rubin, D. B.: Inference from Iterative Simulation Using Multiple Sequences, Stat.
827 Sci., 7(4), 457–472, doi:10.1214/SS/1177011136, 1992.
828 Hanson, P. J., Riggs, J. S., Nettles, W. R., Phillips, J. R., Krassovski, M. B., Hook, L. A., Gu, L.,
829 Richardson, A. D., Aubrecht, D. M., Ricciuto, D. M., Warren, J. M. and Barbier, C.: Attaining
830 whole-ecosystem warming using air and deep-soil heating methods with an elevated CO_2
831 atmosphere, Biogeosciences, 14(4), 861–883, doi:10.5194/bg-14-861-2017, 2017.
832 Hararuk, O., Xia, J. and Luo, Y.: Evaluation and improvement of a global land model against soil
833 carbon data using a Bayesian Markov chain Monte Carlo method, J. Geophys. Res.
834 Biogeosciences, 119(3), 403–417, doi:10.1002/2013JG002535, 2014.
835 Hararuk, O., Smith, M. J. and Luo, Y.: Microbial models with data-driven parameters predict
836 stronger soil carbon responses to climate change, Glob. Chang. Biol., 21(6), 2439–2453,
837 doi:10.1111/gcb.12827, 2015.
838 Hastings, W. K.: Monte carlo sampling methods using Markov chains and their applications,
839 Biometrika, 57(1), 97–109, doi:10.1093/biomet/57.1.97, 1970.
840 Hou, E., Lu, X., Jiang, L., Wen, D. and Luo, Y.: Quantifying Soil Phosphorus Dynamics: A Data
841 Assimilation Approach, J. Geophys. Res. Biogeosciences, 124(7), 2159–2173,
842 doi:10.1029/2018JG004903, 2019.
843 Ise, T. and Moorcroft, P. R.: The global-scale temperature and moisture dependencies of soil

organic carbon decomposition: An analysis using a mechanistic decomposition model, Biogeochemistry, 80(3), 217–231, doi:10.1007/s10533-006-9019-5, 2006.

Iversen, C. M., McCormack, M. L., Powell, A. S., Blackwood, C. B., Freschet, G. T., Kattge, J., Roumet, C., Stover, D. B., Soudzilovskaia, N. A., Valverde-Barrantes, O. J., van Bodegom, P. M. and Violle, C.: A global Fine-Root Ecology Database to address below-ground challenges in plant ecology, New Phytol., 215(1), 15–26, doi:10.1111/nph.14486, 2017.

Jiang, J., Huang, Y., Ma, S., Stacy, M., Shi, Z., Ricciuto, D. M., Hanson, P. J. and Luo, Y.: Forecasting Responses of a Northern Peatland Carbon Cycle to Elevated CO2 and a Gradient of Experimental Warming, J. Geophys. Res. Biogeosciences, 123(3), 1057–1071, doi:10.1002/2017JG004040, 2018.

Kattge, J., Bönisch, G., Díaz, S., Lavorel, S., Prentice, I. C., Leadley, P., Tautenhahn, S., Werner, G. D. A., Aakala, T., Abedi, M., Acosta, A. T. R., Adamidis, G. C., Adamson, K., Aiba, M., Albert, C. H., Alcántara, J. M., Alcázar C, C., Aleixo, I., Ali, H., Amiaud, B., Ammer, C., Amoroso, M. M., Anand, M., Anderson, C., Anten, N., Antos, J., Apgaua, D. M. G., Ashman, T. L., Asmara, D. H., Asner, G. P., Aspinwall, M., Atkin, O., Aubin, I., Baastrup-Spohr, L., Bahalkeh, K., Bahn, M., Baker, T., Baker, W. J., Bakker, J. P., Baldocchi, D., Baltzer, J., Banerjee, A., Baranger, A., Barlow, J., Barneche, D. R., Baruch, Z., Bastianelli, D., Battles, J., Bauerle, W., Bauters, M., Bazzato, E., Beckmann, M., Beeckman, H., Beierkuhnlein, C., Bekker, R., Belfry, G., Belluau, M., Beloiu, M., Benavides, R., Benomar, L., Berdugo-Lattke, M. L., Berenguer, E., Bergamin, R., Bergmann, J., Bergmann Carlucci, M., Berner, L., Bernhardt-Römermann, M., Bigler, C., Bjorkman, A. D., Blackman, C., Blanco, C., Blonder, B., Blumenthal, D., Bocanegra-González, K. T., Boeckx, P., Bohlman, S., Böhning-Gaese, K., Boisvert-Marsh, L., Bond, W., Bond-Lamberty, B., Boom, A., Boonman, C. C. F., Bordin, K.,

867 Boughton, E. H., Boukili, V., Bowman, D. M. J. S., Bravo, S., Brendel, M. R., Broadley, M. R.,
868 Brown, K. A., Bruelheide, H., Brumnich, F., Bruun, H. H., Bruy, D., Buchanan, S. W., Bucher,
869 S. F., Buchmann, N., Buitenwerf, R., Bunker, D. E., et al.: TRY plant trait database – enhanced
870 coverage and open access, Glob. Chang. Biol., 26(1), 119–188, doi:10.1111/gcb.14904, 2020.
871 De Kauwe, M. G., Medlyn, B. E., Walker, A. P., Zaehle, S., Asao, S., Guenet, B., Harper, A. B.,
872 Hickler, T., Jain, A. K., Luo, Y., Lu, X., Luus, K., Parton, W. J., Shu, S., Wang, Y. P., Werner,
873 C., Xia, J., Pendall, E., Morgan, J. A., Ryan, E. M., Carrillo, Y., Dijkstra, F. A., Zelikova, T. J.
874 and Norby, R. J.: Challenging terrestrial biosphere models with data from the long-term
875 multifactor Prairie Heating and CO2 Enrichment experiment, Glob. Chang. Biol., 23(9), 3623–
876 3645, doi:10.1111/gcb.13643, 2017.
877 Keenan, T. F., Davidson, E., Moffat, A. M., Munger, W. and Richardson, A. D.: Using model-data
878 fusion to interpret past trends, and quantify uncertainties in future projections, of terrestrial
879 ecosystem carbon cycling, Glob. Chang. Biol., 18(8), 2555–2569, doi:10.1111/j.1365-
880 2486.2012.02684.x, 2012.
881 Keenan, T. F., Davidson, E. A., Munger, J. W. and Richardson, A. D.: Rate my data: Quantifying
882 the value of ecological data for the development of models of the terrestrial carbon cycle, Ecol.
883 Appl., 23(1), 273–286, doi:10.1890/12-0747.1, 2013.
884 Lawrence, D. M., Fisher, R. A., Koven, C. D., Oleson, K. W., Swenson, S. C., Bonan, G., Collier,
885 N., Ghimire, B., van Kampenhout, L., Kennedy, D., Kluzek, E., Lawrence, P. J., Li, F., Li, H.,
886 Lombardozzi, D., Riley, W. J., Sacks, W. J., Shi, M., Vertenstein, M., Wieder, W. R., Xu, C.,
887 Ali, A. A., Badger, A. M., Bisht, G., van den Broeke, M., Brunke, M. A., Burns, S. P., Buzan, J.,
888 Clark, M., Craig, A., Dahlin, K., Drewniak, B., Fisher, J. B., Flanner, M., Fox, A. M., Gentine,
889 P., Hoffman, F., Keppel-Aleks, G., Knox, R., Kumar, S., Lenaerts, J., Leung, L. R., Lipscomb,

890 W. H., Lu, Y., Pandey, A., Pelletier, J. D., Perket, J., Randerson, J. T., Ricciuto, D. M.,
891 Sanderson, B. M., Slater, A., Subin, Z. M., Tang, J., Thomas, R. Q., Val Martin, M. and Zeng,
892 X.: The Community Land Model Version 5: Description of New Features, Benchmarking, and
893 Impact of Forcing Uncertainty, J. Adv. Model. Earth Syst., 11(12), 4245–4287,
894 doi:10.1029/2018MS001583, 2019.
895 LeBauer, D. S., Wang, D., Richter, K. T., Davidson, C. C. and Dietze, M. C.: Facilitating feedbacks
896 between field measurements and ecosystem models, Ecol. Monogr., 83(2), 133–154,
897 doi:10.1890/12-0137.1, 2013.
898 Levenberg, K.: A method for the solution of certain non-linear problems in least squares, Q. Appl.
899 Math., 2(2), 164–168, 1944.
900 Li, Q., Lu, X., Wang, Y., Huang, X., Cox, P. M. and Luo, Y.: Leaf area index identified as a major
901 source of variability in modeled CO2 fertilization, Biogeosciences, 15(22), 6909–6925,
902 doi:10.5194/bg-15-6909-2018, 2018.
903 Liang, J., Zhou, Z., Huo, C., Shi, Z., Cole, J. R., Huang, L., Konstantinidis, K. T., Li, X., Liu, B.,
904 Luo, Z., Penton, C. R., Schuur, E. A. G., Tiedje, J. M., Wang, Y. P., Wu, L., Xia, J., Zhou, J. and
905 Luo, Y.: More replenishment than priming loss of soil organic carbon with additional carbon
906 input, Nat. Commun., 9(1), 1–9, doi:10.1038/s41467-018-05667-7, 2018a.
907 Liang, J., Zhou, Z., Huo, C., Shi, Z., Cole, J. R., Huang, L., Konstantinidis, K. T., Li, X., Liu, B.,
908 Luo, Z., Penton, C. R., Schuur, E. A. G., Tiedje, J. M., Wang, Y., Wu, L. and Xia, J.: organic
909 carbon with additional carbon input, Nat. Commun., 1–9, doi:10.1038/s41467-018-05667-7,
910 2018b.
911 Lu, D., Ricciuto, D., Walker, A., Safta, C. and Munger, W.: Bayesian calibration of terrestrial
912 ecosystem models: A study of advanced Markov chain Monte Carlo methods, Biogeosciences,

913 14(18), 4295–4314, doi:10.5194/bg-14-4295-2017, 2017.
914 Lu, D., Ricciuto, D., Stoyanov, M. and Gu, L.: Calibration of the E3SM Land Model Using
915 Surrogate-Based Global Optimization, J. Adv. Model. Earth Syst., 10(6), 1337–1356,
916 doi:10.1002/2017MS001134, 2018.
917 Luo, Y. and Schuur, E. A. G.: Model parameterization to represent processes at unresolved scales
918 and changing properties of evolving systems, Glob. Chang. Biol., 26(3), 1109–1117,
919 doi:10.1111/gcb.14939, 2020.
920 Luo, Y., Wu, L., Andrews, J. A., White, L., Matamala, R., Schäfer, K. V. R. and Schlesinger, W.
921 H.: ELEVATED CO2 DIFFERENTIATES ECOSYSTEM CARBON PROCESSES:
922 DECONVOLUTION ANALYSIS OF DUKE FOREST FACE DATA, Ecol. Monogr., 71(3),
923 357–376, doi:10.1890/0012-9615(2001)071[0357:ECDECP]2.0.CO;2, 2001.
924 Luo, Y., Ogle, K., Tucker, C., Fei, S., Gao, C., LaDeau, S., Clark, J. S. and Schimel, D. S.:
925 Ecological forecasting and data assimilation in a data-rich era, Ecol. Appl., 21(5), 1429–1442,
926 doi:10.1890/09-1275.1, 2011.
927 Ma, S., Jiang, J., Huang, Y., Shi, Z., Wilson, R. M., Ricciuto, D., Sebestyen, S. D., Hanson, P. J.
928 and Luo, Y.: Data-Constrained Projections of Methane Fluxes in a Northern Minnesota Peatland
929 in Response to Elevated CO2and Warming, J. Geophys. Res. Biogeosciences, 122(11), 2841–
930 2861, doi:10.1002/2017JG003932, 2017.
931 Metropolis, N., Rosenbluth, A. W., Rosenbluth, M. N., Teller, A. H. and Teller, E.: Equation of
932 state calculations by fast computing machines, J. Chem. Phys., 21(6), 1087–1092,
933 doi:10.1063/1.1699114, 1953.
934 Mitchell, J. C. and Apt, K.: Concepts in programming languages, Cambridge University Press.,
935 2003.

936 Nerger, L. and Hiller, W.: Software for ensemble-based data assimilation systems-Implementation
937 strategies and scalability, Comput. Geosci., 55, 110–118, doi:10.1016/j.cageo.2012.03.026,
938 2013.
939 Van Oijen, M., Cameron, D. R., Butterbach-Bahl, K., Farahbakhshazad, N., Jansson, P. E., Kiese,
940 R., Rahn, K. H., Werner, C. and Yeluripati, J. B.: A Bayesian framework for model calibration,
941 comparison and analysis: Application to four models for the biogeochemistry of a Norway
942 spruce forest, Agric. For. Meteorol., 151(12), 1609–1621, doi:10.1016/j.agrformet.2011.06.017,
943 2011.
944 Ono, S. and Konno, T.: Estimation of flowering date and temperature characteristics of fruit trees by
945 DTS method, Japan Agric. Res. Q., 33(2), 105–108, 1999.
946 Raeder, K., Anderson, J. L., Collins, N., Hoar, T. J., Kay, J. E., Lauritzen, P. H. and Pincus, R.:
947 DART/CAM: An ensemble data assimilation system for CESM atmospheric models, J. Clim.,
948 25(18), 6304–6317, doi:10.1175/JCLI-D-11-00395.1, 2012.
949 Raupach, M. R., Rayner, P. J., Barrett, D. J., Defries, R. S., Heimann, M., Ojima, D. S., Quegan, S.
950 and Schmullius, C. C.: Model-data synthesis in terrestrial carbon observation: Methods, data
951 requirements and data uncertainty specifications, Glob. Chang. Biol., 11(3), 378–397,
952 doi:10.1111/j.1365-2486.2005.00917.x, 2005.
953 Rayner, P. J., Scholze, M., Knorr, W., Kaminski, T., Giering, R. and Widmann, H.: Two decades of
954 terrestrial carbon fluxes from a carbon cycle data assimilation system (CCDAS), Global
955 Biogeochem. Cycles, 19(2), n/a-n/a, doi:10.1029/2004GB002254, 2005.
956 Ricciuto, D., Sargsyan, K. and Thornton, P.: The Impact of Parametric Uncertainties on
957 Biogeochemistry in the E3SM Land Model, J. Adv. Model. Earth Syst., 10(2), 297–319,
958 doi:10.1002/2017MS000962, 2018.

959 Ricciuto, D. M., King, A. W., Dragoni, D. and Post, W. M.: Parameter and prediction uncertainty in
960 an optimized terrestrial carbon cycle model: Effects of constraining variables and data record
961 length, J. Geophys. Res., 116(G1), G01033, doi:10.1029/2010JG001400, 2011.
962 Richardson, A. D., Williams, M., Hollinger, D. Y., Moore, D. J. P., Dail, D. B., Davidson, E. A.,
963 Scott, N. A., Evans, R. S., Hughes, H., Lee, J. T., Rodrigues, C. and Savage, K.: Estimating
964 parameters of a forest ecosystem C model with measurements of stocks and fluxes as joint
965 constraints, Oecologia, 164(1), 25–40, doi:10.1007/s00442-010-1628-y, 2010.
966 Richardson, A. D., Hufkens, K., Milliman, T., Aubrecht, D. M., Chen, M., Gray, J. M., Johnston,
967 M. R., Keenan, T. F., Klosterman, S. T., Kosmala, M., Melaas, E. K., Friedl, M. A. and Frolking,
968 S.: Tracking vegetation phenology across diverse North American biomes using PhenoCam
969 imagery, Sci. Data, 5, 1–24, doi:10.1038/sdata.2018.28, 2018.
970 Ridler, M. E., Van Velzen, N., Hummel, S., Sandholt, I., Falk, A. K., Heemink, A. and Madsen, H.:
971 Data assimilation framework: Linking an open data assimilation library (OpenDA) to a widely
972 adopted model interface (OpenMI), Environ. Model. Softw., 57, 76–89,
973 doi:10.1016/j.envsoft.2014.02.008, 2014.
974 Robert, C. and Casella, G.: Monte Carlo statistical methods, Springer Science & Business Media.,
975 2013.
976 Roberts, G. O., Gelman, A. and Gilks, W. R.: Weak convergence and optimal scaling of random
977 walk Metropolis algorithms, Ann. Appl. Probab., 7(1), 110–120,
978 doi:10.1214/AOAP/1034625254, 1997.
979 Safta, C., Ricciuto, D. M., Sargsyan, K., Debusschere, B., Najm, H. N., Williams, M. and Thornton,
980 P. E.: Global sensitivity analysis, probabilistic calibration, and predictive assessment for the data
981 assimilation linked ecosystem carbon model, Geosci. Model Dev., 8(7), 1899–1918,

982 doi:10.5194/gmd-8-1899-2015, 2015.
983 Scholze, M., Kaminski, T., Rayner, P., Knorr, W. and Giering, R.: Propagating uncertainty through
984 prognostic carbon cycle data assimilation system simulations, J. Geophys. Res., 112(D17),
985 D17305, doi:10.1029/2007JD008642, 2007.
986 Shi, Z., Crowell, S., Luo, Y. and Moore, B.: Model structures amplify uncertainty in predicted soil
987 carbon responses to climate change, Nat. Commun., 9(1), 1–11, doi:10.1038/s41467-018-04526-
988 9, 2018.
989 Smith, M. J., Purves, D. W., Vanderwel, M. C., Lyutsarev, V. and Emmott, S.: The climate
990 dependence of the terrestrial carbon cycle, including parameter and structural uncertainties,
991 Biogeosciences, 10(1), 583–606, doi:10.5194/bg-10-583-2013, 2013.
992 Strigul, N., Pristinski, D., Purves, D., Dushoff, J. and Pacala, S.: Scaling from trees to forests:
993 Tractable macroscopic equations for forest dynamics, Ecol. Monogr., 78(4), 523–545,
994 doi:10.1890/08-0082.1, 2008.
995 Tao, F., Zhou, Z., Huang, Y., Li, Q., Lu, X., Ma, S., Huang, X., Liang, Y., Hugelius, G., Jiang, L.,
996 Doughty, R., Ren, Z. and Luo, Y.: Deep Learning Optimizes Data-Driven Representation of Soil
997 Organic Carbon in Earth System Model Over the Conterminous United States, Front. Big Data,
998 3(June), 1–15, doi:10.3389/fdata.2020.00017, 2020.
999 Trudinger, C. M., Raupach, M. R., Rayner, P. J., Kattge, J., Liu, Q., Park, B., Reichstein, M.,
1000 Renzullo, L., Richardson, A. D., Roxburgh, S. H., Styles, J., Wang, Y. P., Briggs, P., Barrett, D.
1001 and Nikolova, S.: OptIC project: An intercomparison of optimization techniques for parameter
1002 estimation in terrestrial biogeochemical models, J. Geophys. Res. Biogeosciences, 112(2), 1–17,
1003 doi:10.1029/2006JG000367, 2007.
1004 Wang, Y. P., Trudinger, C. M. and Enting, I. G.: A review of applications of model-data fusion to

1005 studies of terrestrial carbon fluxes at different scales, Agric. For. Meteorol., 149(11), 1829–1842,
1006 doi:10.1016/j.agrformet.2009.07.009, 2009.
1007 Weng, E. and Luo, Y.: Relative information contributions of model vs. data to short- and long-term
1008 forecasts of forest carbon dynamics, Ecol. Appl., 21(5), 1490–1505, doi:10.1890/09-1394.1,
1009 2011.
1010 Weng, E., Dybzinski, R., Farrior, C. E. and Pacala, S. W.: Competition alters predicted forest
1011 carbon cycle responses to nitrogen availability and elevated CO_2: simulations using an explicitly
1012 competitive, game-theoretic vegetation demographic model, Biogeosciences Discuss., 1–35,
1013 doi:10.5194/bg-2019-55, 2019.
1014 Williams, M., Schwarz, P. A., Law, B. E., Irvine, J. and Kurpius, M. R.: An improved analysis of
1015 forest carbon dynamics using data assimilation, Glob. Chang. Biol., 11(1), 89–105,
1016 doi:10.1111/j.1365-2486.2004.00891.x, 2005.
1017 Williams, M., Richardson, A. D., Reichstein, M., Stoy, P. C., Peylin, P., Verbeeck, H., Carvalhais,
1018 N., Jung, M., Hollinger, D. Y., Kattge, J., Leuning, R., Luo, Y., Tomelleri, E., Trudinger, C. M.
1019 and Wang, Y. P.: Improving land surface models with FLUXNET data, Biogeosciences, 6(7),
1020 1341–1359, doi:10.5194/bg-6-1341-2009, 2009.
1021 Xu, T., White, L., Hui, D. and Luo, Y.: Probabilistic inversion of a terrestrial ecosystem model:
1022 Analysis of uncertainty in parameter estimation and model prediction, Global Biogeochem.
1023 Cycles, 20(2), 1–15, doi:10.1029/2005GB002468, 2006.
1024 Yun, K., Hsiao, J., Jung, M. P., Choi, I. T., Glenn, D. M., Shim, K. M. and Kim, S. H.: Can a multi-
1025 model ensemble improve phenology predictions for climate change studies?, Ecol. Modell., 362,
1026 54–64, doi:10.1016/j.ecolmodel.2017.08.003, 2017.
1027 Zobitz, J. M., Desai, A. R., Moore, D. J. P. and Chadwick, M. A.: A primer for data assimilation

with ecological models using Markov Chain Monte Carlo (MCMC), Oecologia, 167(3), 599–611, doi:10.1007/s00442-011-2107-9, 2011.

Table1: Comparison among MIDA and available DA tools

DA tool	Agnostic	DA algorithms	Global optima	Posterior distribution	Visualization
CCDAS	No	Automatic differentiation from Transformation of Algorithms in Fortran (TAF)	No	No	No
CARDAMOM	No	Markov Chain Monte Carlo	Yes	Yes	No
EcoPAD	No	Markov Chain Monte Carlo	Yes	Yes	Yes
OpenDA	No	EnKF, Ensemble Square-Root Filter, Particle Filter	Yes	Yes	No
DART	Yes	EnKF	Yes	Yes	No
PDAF	Yes	EnKF	Yes	Yes	No
PEST	Yes	Levenberg-Marquardt method	Rely on initial parameter values	No	No
MIDA	Yes	Markov Chain Monte Carlo	Yes	Yes	Yes

Table 2: A summary of 21 parameters to be calibrated in DALEC model. The default parameter value and prior parameter range are shown.

Parameter	Description	Unit	Default	Range
GDD_{min}	Growing degree day threshold for leaf out	$^{o}C\ d$	100	[10, 250]
GDD_{max}	Growing degree day threshold for maximum LAI	$^{o}C\ d$	200	[50, 500]
LAI_{max}	Seasonal maximum leaf area index	-	4	[2, 7]
$T_{leaffall}$	Temperature for leaf fall	^{o}C	5	[0, 10]
K_{leaf}	Rate of leaf fall	d^{-1}	0.1	[0.03 0.95]
NUE	N use efficiency	-	7	[1, 20]
Res_{growth}	Growth respiration fraction	-	0.2	[0.05, 0.5]
Res_{m}	Base rate for maintenance respiration	$\times 10^{-4}\ \mu mol\ m^{-2}d^{-1}$	1	$[0.1, 100]$
$Q_{10_{mr}}$	Maintenance respiration T-sensitivity	-	2	[1, 4]
A_{stem}	Allocation to plant stem pool	-	0.7	[0.1, 0.95]
τ_{root}	Root turnover time	$\times 10^{-4}\ d^{-1}$	5.48	$[1.1, 27.4]$
τ_{stem}	Stem turnover time	$\times 10^{-5}\ d^{-1}$	5.48	$[1.1, 27.4]$
$Q_{10_{hr}}$	Heterotrophic respiration T-sensitivity	-	2	[1, 4]
τ_{litter}	Base turnover for litter	$\times 10^{-3}\ umol\ m^{-2}d^{-1}$	1.37	$[0.548, 5.48]$
τ_{som}	Base turnover for soil organic matter	$\times 10^{-4}\ umol\ m^{-2}d^{-1}$	9.13	$[0.274, 2.74]$
K_{decomp}	Decomposition rate	$\times 10^{-3}\ d^{-1}$	1	$[0.1, 10]$
LMA	Leaf mass per area	$gC\ m^{-2}$	80	[20, 150]
$X_{stem_{init}}$	Initial value for stem C pool	$\times 10^{3}\ gC$	5	$[1, 15]$
$X_{root_{init}}$	Initial value for root C pool	gC	500	[100, 3000]
$X_{litter_{init}}$	Initial value for litter C pool	gC	600	[50, 1000]
$X_{som_{init}}$	Initial value for soil organic C pool	$\times 10^{3}\ gC$	7	[1, 25]

Table 3: A summary of eight parameters to be calibrated in surrogate-based ELM model. The default parameter value and prior parameter range are shown.

Parameter	Description	Unit	Default	Range
c_{root}	Rooting depth distribution parameter	m^{-1}	2.0	$[0.5, 4]$
SLA_{top}	Specific leaf area at canopy top	$m^2 gC^{-1}$	0.03	$[0.01, 0.05]$
N_{leaf}	Fraction of leaf N in RuBisCO	-	0.1007	$[0.1, 0.4]$
CN_{root}	Fine root C:N ratio	-	42	$[25, 60]$
A_{r2l}	Allocation ratio of fine root to leaf	-	1.0	$[0.3, 1.5]$
Res_m	Base rate for maintenance respiration	$\times 10^{-6} \mu mol\ m^{-2} s^{-1}$	2.525	$[1.5, 4]$
$t_{leaffall}$	Critical day length for senescence	$\times 10^4$ s	3.93	$[3.5, 4.5]$
GDD_{onset}	Accumulated growing degree days for leaf out	$^oC\ d$	800	$[600, 1000]$

Table 4: A summary of two parameters to be calibrated in the BiomE model. The default parameter value and prior parameter range are shown.

Parameter	Description	Unit	Default	Range
V_{annual}	Annual productivity per unit leaf area	$kgC\ y^{-1}m^2$	0.4	$[0.2, 2]$
M_{canopy}	Annual mortality rate in canopy layer	y^{-1}	0.02	$[0.01, 0.08]$

Figure captions

Figure 1: The three-step workflow of Model Independent Data Assimilation (MIDA) module. The workflow includes data preparation, execution of data assimilation (DA), and visualization. The data preparation step is to provide all the formatted essential data for DA via user input. The execution step is to calibrate parameter values towards a constrained posterior distribution with the fusion of observations. The visualization step is to diagnose the effects of DA. Rhombus in orange represents user-input data. Rectangle represents procedures and document/multidocument shape is for data files in computers. Dashed lines indicate locations of data. Solids lines indicate data flow pathways. With the three-step workflow, DA is agnostic to specific models and users will be released from technical burdens.

Figure 2: the GUI-MIDA window includes two panels. The upper panel is to set up a data assimilation task. Inputs can be loaded and applied to the step 1 on data preparation for DA. The lower panel is to run DA as described in step 2 and visualize the posterior distributions of parameters in step 3.

Figure 3: Comparison between the simulated daily net ecosystem exchange (NEE) by DALEC and the observed NEE at Harvard Forest from 1992 to 2006. Red circles represent modeled NEE with the optimized parameter values and green circles represent simulated NEE with the original parameter values. Simulations of DALEC are substantially improved after data assimilation in comparison with those before data assimilation.

Figure 4: Comparison between posterior distributions (red line) and default values (gray dash line) of the 21 parameters in DALEC. The peak in posterior distribution is the constrained parameter value from maximum likelihood estimation. This distinctive mode and its divergence from the default value indicates the effects of DA. Most parameters are well constrained, and some are far different from the original values.

Figure 5: Comparison between posterior distributions (red line) and default values (gray dash line) of the eight parameters in surrogate-based ELM. The peak in posterior distribution is the constrained parameter value from maximum likelihood estimation. This distinctive mode and its divergence from the default value indicates the effects of DA. Most parameters are well constrained, and some are far different from the original values.

Figure 6: Comparison between the simulated NEE, total leaf area index, latent heat flux by surrogate-based ELM and the observed ones at Missouri Ozark flux site from 2006 to 2014. The

blue lines indicate the observations, and their 95% confidence interval is in the dashed area. The green and red lines indicate the simulations with default parameter values and optimized values respectively. Simulations are generally improved after DA for all these three variables.

Figure 7: Comparison between the simulated growth date by 9 phenology models after DA and the observed growth date for *Larix laricina* with +9°C treatment at SPRUCE site from 2016 to 2018. Colored number indicates different models and shape represents different year. Overall, model 6,7,8,9 achieve better performance after DA.

Figure 8: Comparison between posterior distributions (red line) and default values (gray dash line) of the two parameters in BiomeE. The peak in posterior distribution is the constrained parameter value from maximum likelihood estimation. This distinctive mode and its divergence from the default value indicates the effects of DA. All parameters are well constrained and different from their original values.

Figure 9: Comparison between the simulated leaf area index (LAI) by BiomeE and the observed NEE at Willow Creek. Circles represent modeled NEE with the optimized parameter values and triangles represent simulated NEE with the original parameter values. Simulations of LAI are substantially improved after data assimilation in comparison with those before data assimilation.

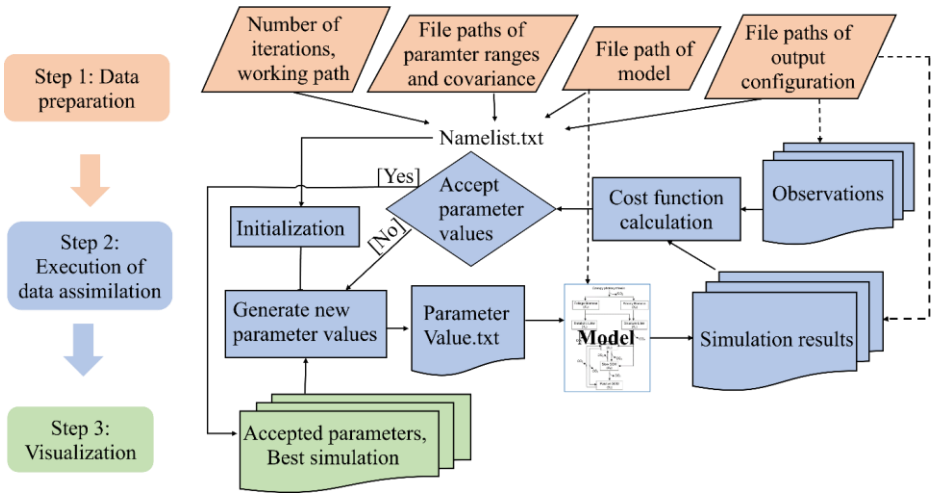

Figure 1: The three-step workflow of Model Independent Data Assimilation (MIDA) module. The workflow includes data preparation, execution of data assimilation (DA), and visualization. The data preparation step is to provide all the formatted essential data for DA via user input. The execution step is to calibrate parameter values towards a constrained posterior distribution with the fusion of observations. The visualization step is to diagnose the effects of DA. Rhombus in orange represents user-input data. Rectangle represents procedures and document/multidocument shape is for data files in computers. Dashed lines indicate locations of data. Solids lines indicate data flow pathways. With the three-step workflow, DA is agnostic to specific models and users will be released from technical burdens.

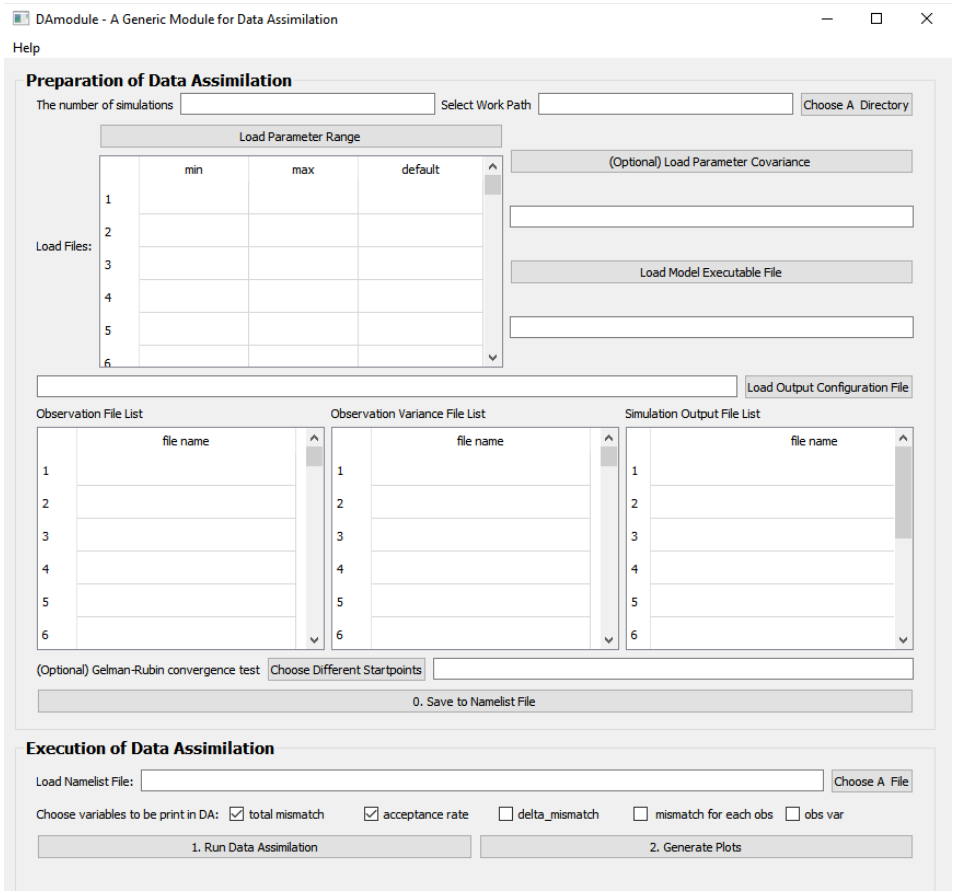

Figure 2: the GUI-MIDA window includes two panels. The upper panel is to set up a data assimilation task. Inputs can be loaded and applied to the step 1 on data preparation for DA. The lower panel is to run DA as described in step 2 and visualize the posterior distributions of parameters in step 3.

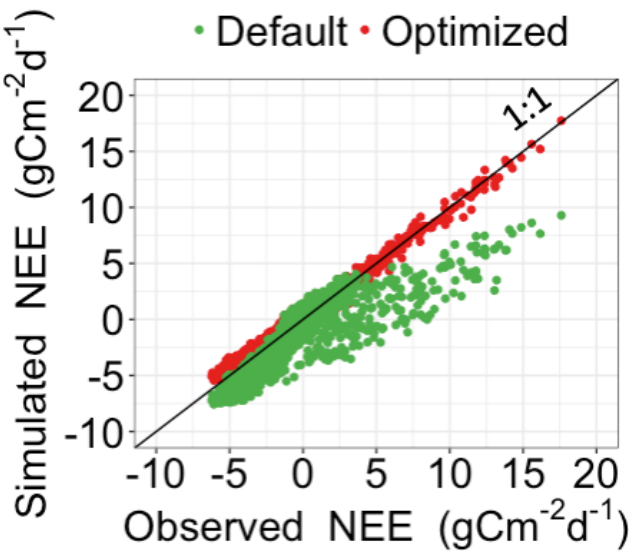

Figure 3: Comparison between the simulated daily net ecosystem exchange (NEE) by DALEC and the observed NEE at Harvard Forest from 1992 to 2006. Red circles represent modeled NEE with the optimized parameter values and green circles represent simulated NEE with the original parameter values. Simulations of DALEC are substantially improved after data assimilation in comparison with those before data assimilation.

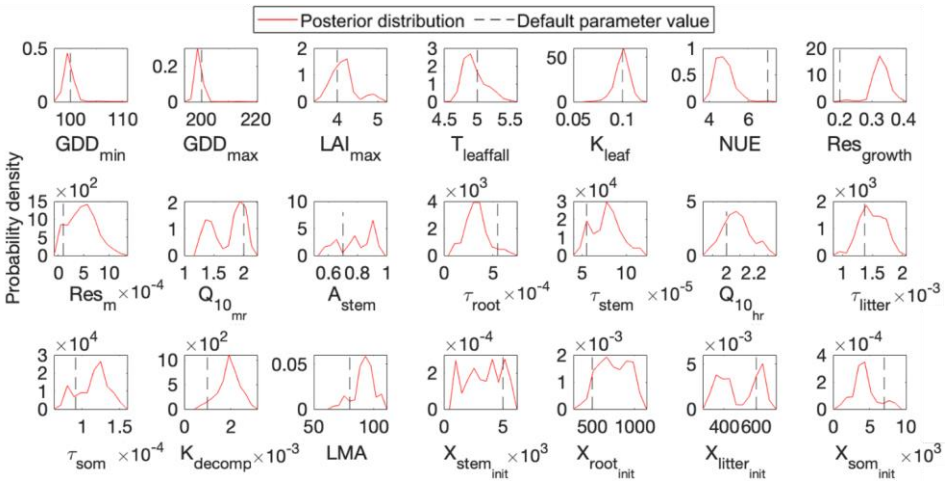

Figure 4: Comparison between posterior distributions (red line) and default values (gray dash line) of the 21 parameters in DALEC. The peak in posterior distribution is the constrained parameter value from maximum likelihood estimation. This distinctive mode and its divergence from the default value indicates the effects of DA. Most parameters are well constrained, and some are far different from the original values.

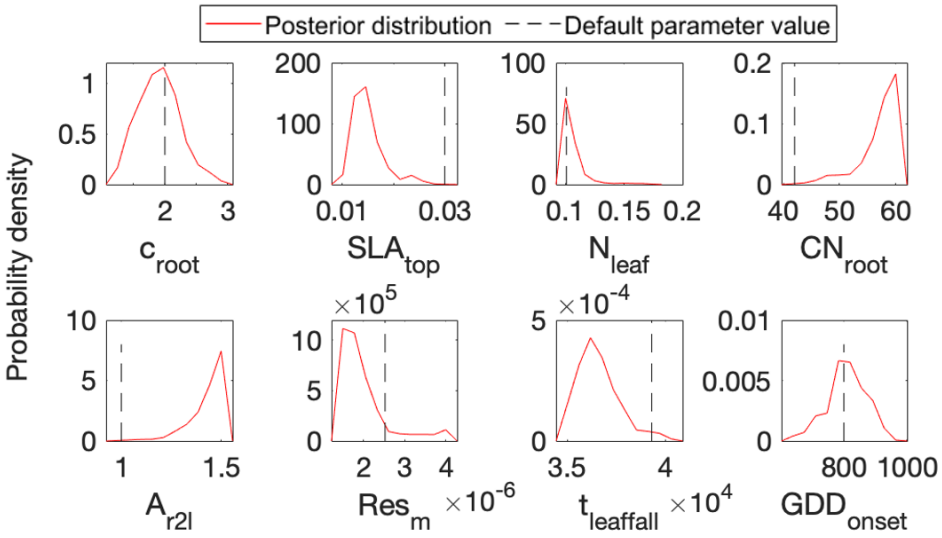

Figure 5: Comparison between posterior distributions (red line) and default values (gray dash line) of the eight parameters in surrogate-based ELM. The peak in posterior distribution is the constrained parameter value from maximum likelihood estimation. This distinctive mode and its divergence from the default value indicates the effects of DA. Most parameters are well constrained, and some are far different from the original values.

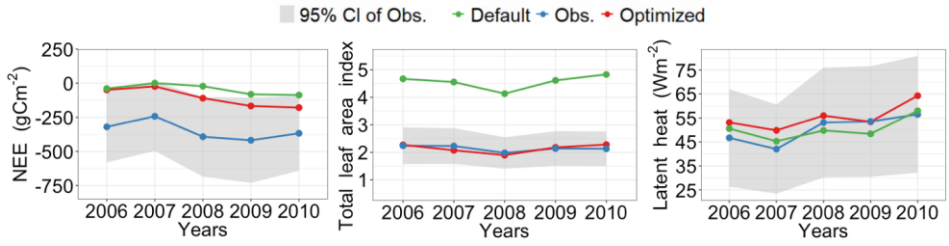

Figure 6: Comparison between the simulated NEE, total leaf area index, latent heat flux by surrogate-based ELM and the observed ones at Missouri Ozark flux site from 2006 to 2014. The blue lines indicate the observations, and their 95% confidence interval is in the dashed area. The green and red lines indicate the simulations with default parameter values and optimized values respectively. Simulations are generally improved after DA for all these three variables.

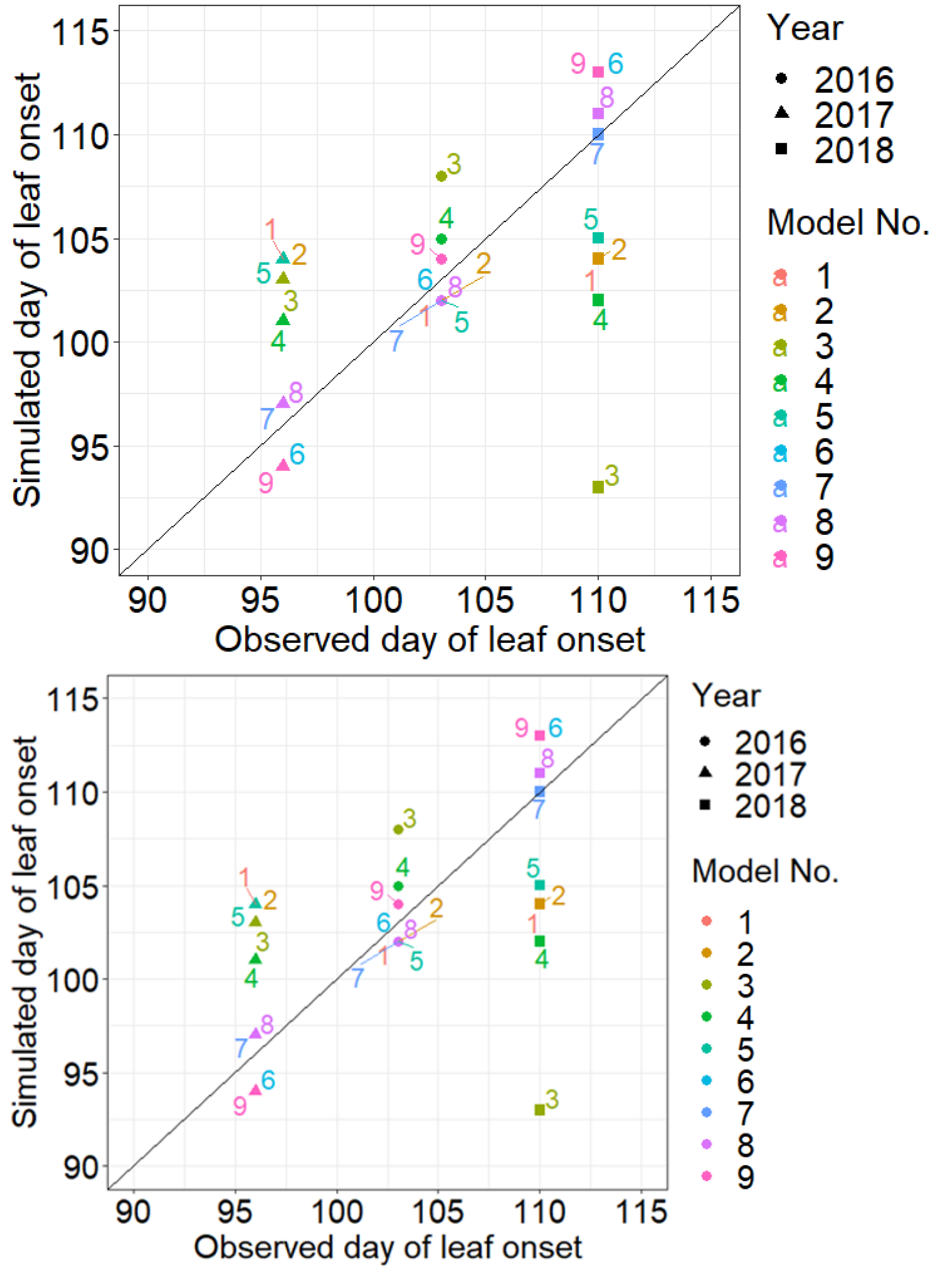
Simulated day of leaf onset
Observed day of leaf onset
90
95
100
105
110
115
Year
2016
2017
2018
Model No.
1
2
3
4
5
6
7
8
9

Figure 7: Comparison between the simulated growth date by 9 phenology models after DA and the observed growth date for *Larix laricina* with +9℃ treatment at SPRUCE site from 2016 to 2018. Colored number indicates different models and shape represents different year. Overall, model 6,7,8,9 achieve better performance after DA.

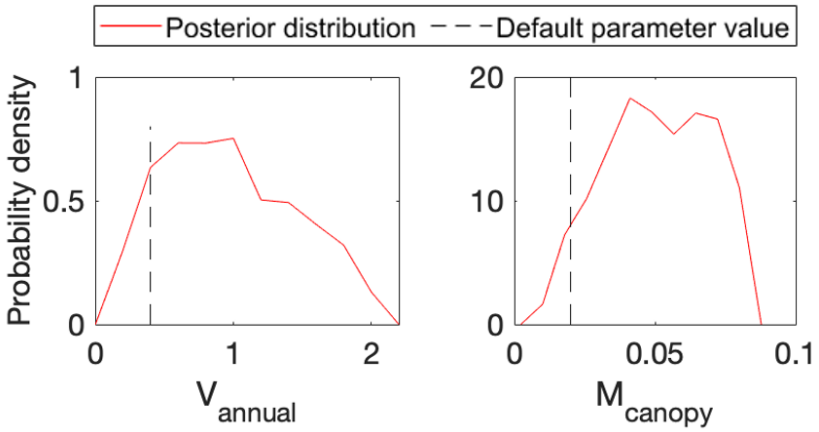

Figure 8: Comparison between posterior distributions (red line) and default values (gray dash line) of the two parameters in BiomeE. The peak in posterior distribution is the constrained parameter value from maximum likelihood estimation. This distinctive mode and its divergence from the default value indicates the effects of DA. All parameters are well constrained and different from their original values.

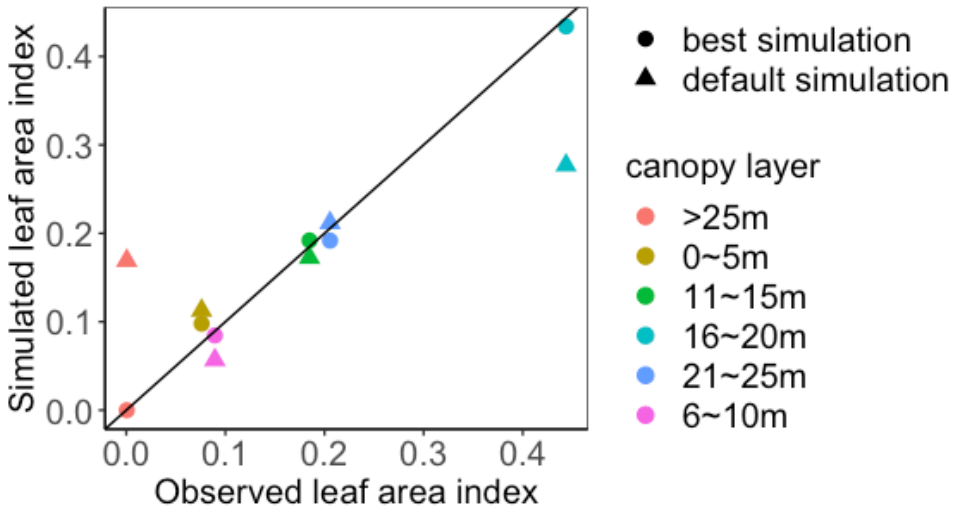

Figure 9: Comparison between the simulated leaf area index (LAI) by BiomeE and the observed NEE at Willow Creek. Circles represent modeled NEE with the optimized parameter values and triangles represent simulated NEE with the original parameter values. Simulations of LAI are substantially improved after data assimilation in comparison with those before data assimilation.